Systematic Photonic Crystal Device Design: Global and Local Optimization and Sensitivity Analysis

Yang Jiao, *Member, IEEE*, Shanhui Fan, and David A. B. Miller, *Fellow, IEEE*

***Abstract*—We present a set of modeling, sensitivity analysis, and design optimization methods for photonic crystal structures based on Wannier basis field expansion and efficient matrix analysis techniques. We develop the sensitivity analysis technique to analyze both refractive index perturbations and dielectric boundary shift perturbations. Our modeling method is $\sim 1000\times$ faster than finite-difference time-domain (FDTD) for searching through a large number of similar device designs. We show that our optimization techniques, relying on the efficiency of the modeling and sensitivity analysis methods, enable systematic global and local optimizations of integrated optical components. We show that our design method can be controlled to favor designs without high-energy build-ups, potentially making them more fabrication-error tolerant. We present design examples and verify our designs with FDTD calculations.**

***Index Terms*—Bragg scattering, design automation, design methodology, electromagnetic scattering by periodic structures, integrated optics, optical propagation in nonhomogeneous media, optimization methods, periodic structures, photonic crystals, Wannier functions.**

I. Introduction

PHOTONIC CRYSTAL (PC) devices are finding applications in many areas of optics and optoelectronics. As a result there is an increasing demand for better PC device analysis and design tools. Finite-difference time-domain (FDTD) [1] simulation has become a reliable analysis tool, but it remains computationally expensive for most personal computers. Efficient plane wave-based eigenmode solvers (PWM) [2] are greatly simplifying the analysis of PC materials and aiding resonator designs, but they fail short of supporting analysis of large arbitrary PC devices. PC device analysis thus remains a computationally expensive process. Furthermore, there has been no method available for efficiently and systematically *designing* PC devices. Even though physical insights and innovative modeling provide guidelines when designing PC devices, the majority of PC device designs still require tedious trial and error fine tuning [3], [4]. The fine-tuning is particularly tedious because the standard analysis tools are not fast enough and their computational cost scales badly with device size. In this paper, we introduce a set of new design, optimization, and sensitivity analysis methods for PC devices. The methods are based on Wannier basis analysis of the device, and on efficient matrix analysis techniques that make design optimization and sensitivity analysis computationally inexpensive. Our design optimization method allows one to design PC devices that satisfy arbitrary transmission/reflection characteristics using modest personal computational hardware. Analysis of performance changes due to perturbations, such as fabrication error and temperature induced index change, is an important step for PC structure design. Our Wannier basis gradient (WBG) sensitivity analysis method allows one to calculate the effect of perturbations with unprecedented speed and efficiency.

Due to the limitations and inefficiencies of FDTD and PWM, various authors have worked on more efficient methods of analyzing PC devices. Multiple-multipole methods [5], [6] expand the field in cylindrical or vector spherical harmonics, and are very efficient at analyzing PC structures made of dielectric cylinders or spheres. However, the method cannot be generalized for arbitrary unit cells. Transfer matrix methods have been successfully generalized to treat wave propagation in layers of PC materials [7]. However, because the method treats PC devices as stacks of materials, supercell calculations must be used in conjunction to handle waveguide structures. This greatly increases the computational complexity of the method for large structures.

To perform sensitivity analysis on PC strucutre, the standard finite difference approach is to solve for the performance parameters before and after perturbations. Often, computationally expensive FDTD or PWM simulations need to be repeated for each perturbation scenario. An emerging technique, the finite-difference frequency-domain (FDFD) sensitivity analysis method [8], is much more efficient. The method works very well for arbitrary dielectric structures, not just periodic media. Our WBG method, after a set of initial calculations, is optimized for each particular PC. To analyze multiple designs in the same PC, it is more efficient to use the WBG method for sensitivity analysis than FDFD.

Wannier functions were first used to study quantum mechanical systems in solid state physics. Wannier functions are unitary transforms of the Bloch functions of any periodic system, including PCs. Like the Bloch functions, the Wannier functions form a complete basis for analyzing fields. Unlike the Bloch functions, however, the Wannier functions are localized, i.e., they decay to zero rapidly away from a center point. The localization of the Wannier basis makes them ideal for analyzing PC defect structures with localized fields. Taking advantage of the arbitrary phase that can be assigned to the Bloch functions when constructing the Wannier basis, Marzari [9] developed a method to maximize the localization of the resulting Wannier basis. Since then, Busch and many researchers [10], [11] have

Manuscript received July 15, 2005; revised October 11, 2005.

Y. Jiao is with Intel Corporation, Santa Clara, CA 95054 USA (e-mail: jiaoyang@stanfordalumni.org).

S. Fan and D. A. B. Miller are with the Ginzton Laboratory, Stanford University, Stanford, CA 94305-4088 USA (e-mail: shanhui@stanford.edu; dabm@ee.stanford.edu).

Digital Object Identifier 10.1109/JQE.2005.862038

worked on constructing maximally localized Wannier bases for PCs and have introduced methods for analyzing PC structures in such a basis. The full power of the Wannier basis representation, however, has yet to be exploited in constructing a *design and optimization* method for PC defect structures. The core of this paper is to develop such a method, and we will show that it enables the design of extremely compact PC devices with complex functionalities.

Our design, optimization, and sensitivity analysis methods all involve a one-time evaluation of a few small perturbation matrices associated with modifications made to a particular single unit cell in a PC. The perturbation matrices for the same modification applied to different unit cells or multiple unit cells are then obtained by trivial matrix additions and shifts of the single-unit cell perturbation matrices. Furthermore, the same matrices can be used for different devices constructed in the same PC. After obtaining the perturbation matrices, both the design and optimization method and the sensitivity analysis method only involve a few computationally trivial matrix multiplications. As a result, in contrast to FDTD and PWM methods, our methods can be used to design and analyze large PC devices (hundreds of lattice sites) on personal computers. Also compared to FDTD and PWM, the new methods do not require finer computational grids for smaller dielectric boundary perturbations.

We have presented a brief outline of our design and optimization method for two-dimensional (2-D) scalar fields with isotropic, nonmagnetic materials in [12]. In this paper, we review Wannier basis EM analysis and develop our design and optimization method in the general framework of three-dimensional (3-D) vector fields, and general permittivity and permeablity tensors for the PC and for the defects. In [13], we have outlined our sensitivity analysis method for scalar fields. In this paper, we present a method for resolving the difficulties in applying the sensitivity analysis to shifts in discontinuous dielectric boundaries when we are dealing with vector fields. This paper is self-contained and presents thorough derivations of the design, optimization, and sensitivity analysis equations.

In addition, we will introduce a local optimization algorithm that takes advantage of both the design method and the sensitivity analysis method. Our previous design method is a global optimization algorithm that finds a good design using a heuristic search. We will show that the new local optimization algorithm can be used to fine-tune designs obtained by the previous method either to further improve the performance or to optimize secondary characteristics of the design.

We demonstrate our design paradigm with a design of an extremely compact mode demultiplexer. The device separates the three modes of the input waveguide and converts them into the modes of three output single mode waveguides. As the example will show, the method works even when there is very little physical intuition to guide the design. We will demonstrate the application of our sensitivity analysis method to transmission type structures as well as resonator structures, and verify the results with FDTD and PWM supercell simulations.

Lastly, we will demonstrate design refinements of the mode demultiplexer with two approaches. First, we show the design can be easily improved if we allow a tradeoff of device area with device performance. We show that the Wannier basis low rank update allows us to enlarge a device, increase the transmission, while maintaining the operation bandwidth. Second we apply our new localized optimization method to improve the transmission efficiency of the mode demultiplexer design. The new method improved the peak transmission of the device from 90% to near unity. We verify the result with FDTD simulations.

In the next section, we will start with the formulation of the wave equation in the Wannier basis for PC defect structures. In Section III, we will present the theory behind systematic design of PC devices using small rank adjustments. Next, in Section IV, we will present our sensitivity analysis method for both transmission type structures and resonator structures. We will elaborate in that section on the application of the sensitivity analysis method to shifting material boundaries. In Section V, we present the new Wannier basis local optimization algorithm. In Section VI, we present numerical examples of the methods and results of the new local optimization algorithm. We conclude in Section VII.

II. Maxwell Equations on a Wannier Basis

A. Vector Wave Equation in the Wannier Basis for PC Defects

In this paper, we will use lower case bold symbols, such as $\boldsymbol{r}$, to denote vectors. Upper case bold symbols, such as $\mathbf{M}$, will denote matrices. Underlined letters, such as $\underline{\varepsilon}$, will denote tensor quantities. We denote the perfectly periodic PC by the lossless permittivity and permeability tensors $\underline{\varepsilon}_p(\boldsymbol{r})$ and $\underline{\mu}_p(\boldsymbol{r})$. Assuming a monochromatic field and a linear medium, the source-free Maxwell's equations for the E-field lead to the eigenequations for the periodic system

$$\nabla \times \underline{\mu}_p(\boldsymbol{r})^{-1} \nabla \times E_n(k, \boldsymbol{r}) = \omega_n^2(\boldsymbol{k}) \underline{\varepsilon}_p(\boldsymbol{r}) E_n(\boldsymbol{k}, \boldsymbol{r}) \tag{1}$$

where $\boldsymbol{E}_n(\boldsymbol{k}, r)$ are the Bloch waves indexed by band n and wavevector $\boldsymbol{k}(\omega)$. The Bloch waves form a complete basis for physical fields in PC devices. A device in this PC can be described by the perturbed tensors

$$\begin{aligned} \underline{\varepsilon}(\boldsymbol{r}) &= \underline{\varepsilon}_p(\boldsymbol{r}) + \underline{\varepsilon}_\Delta(\boldsymbol{r}) \\ \underline{\mu}(\boldsymbol{r}) &= \underline{\mu}_p(\boldsymbol{r}) + \underline{\mu}_\Delta(\boldsymbol{r}) \end{aligned}$$

where $\underline{\varepsilon}_\Delta(\boldsymbol{r})$ and $\underline{\mu}_\Delta(\boldsymbol{r})$ represent defects in the otherwise periodic material. For later convenience, we write the inverse of the permeability tensor as

$$\begin{aligned} \underline{\mu}^{-1} &= \underline{\mu}_p^{-1} - [\underline{\mu}_p(\underline{\mu}_\Delta)^{-1}\underline{\mu}_p + \underline{\mu}_p]^{-1} \\ &\equiv \underline{\mu}_p^{-1} - \underline{\eta}_\Delta^{-1} \end{aligned} \tag{2}$$

where we have defined the perturbation to $\underline{\mu}_p^{-1}$ as $\underline{\eta}_\Delta^{-1}$. For the device, we have

$$\nabla \times \underline{\mu}(\boldsymbol{r})^{-1} \nabla \times \boldsymbol{E}(\boldsymbol{r}) = \omega^2 \underline{\varepsilon}(\boldsymbol{r}) \boldsymbol{E}(\boldsymbol{r}) \tag{3}$$

where $\boldsymbol{E}(\boldsymbol{r})$ is the electric field vector, and ω is the frequency. To solve for the steady state field $\boldsymbol{E}(\boldsymbol{r})$ for a particular device, we make use of the Wannier basis functions. The maximally

localized Wannier functions $\boldsymbol{W}_{n,\boldsymbol{R}}(\boldsymbol{r})$ are defined by the lattice transform of the Bloch wave basis [9]

$$\boldsymbol{W}_{n,\boldsymbol{R}}(\boldsymbol{r}) \equiv \frac{\Omega}{(2\pi)^3} \int_{\mathrm{BZ}} d\boldsymbol{k} e^{-i\boldsymbol{k}\cdot\boldsymbol{R}} \sum_m \left[\mathbf{U}^{(\boldsymbol{k})}_{n,m}\right] \boldsymbol{E}_m(\boldsymbol{k},\boldsymbol{r}) \quad (4)$$

where Ω is the unit cell volume, $\boldsymbol{R}$ is a real space lattice vector, $\mathbf{U}^{(\boldsymbol{k})}_{n,m}$ are elements of the unitary transform matrix $\mathbf{U}^{(\boldsymbol{k})}$ that mixes the Bloch functions from different PC bands, and the integration is over the first Brillouin zone. The inverse relation is

$$\boldsymbol{E}_n(\boldsymbol{k},\boldsymbol{r}) = \sum_{\boldsymbol{R}} e^{i\boldsymbol{k}\cdot\boldsymbol{R}} \sum_m \left[\mathbf{U}^{\dagger(\boldsymbol{k})}_{n,m}\right] \boldsymbol{W}_{m,\boldsymbol{R}}(\boldsymbol{r}). \quad (5)$$

Now we expand the E-field in the Wannier basis as

$$\boldsymbol{E}(\boldsymbol{r}) = \sum_{n,\boldsymbol{R}} b_{n,\boldsymbol{R}} \boldsymbol{W}_{n,\boldsymbol{R}}(\boldsymbol{r}) \quad (6)$$

where $b_{n,\boldsymbol{R}}$ are the expansion coefficients. The Wannier basis is a very efficient basis, in the sense that a relatively small number of expansion coefficients is sufficient to accurately represent typical fields in a PC structure. Various works have studied the wave equation in the Wannier basis for structures with dielectric constant perturbations in both E-field and H-field [10], [14]. In particular, Busch [10] presented a Wannier basis formalism for analyzing PC structures with dielectric constant defects. For the more complete case of vector fields, when *both* dielectric constant defects and magnetic permittivity defects are present, we show (see Appendix A) that the source-free wave equation can be written in the form

$$[\omega^{-2}\mathbf{B} - \mathbf{D}]\mathbf{b} = [\mathbf{I} - \omega^{-2}\mathbf{A}]\mathbf{b} \quad (7)$$

where $\mathbf{b}$ is the vector of Wannier basis coefficients and $\mathbf{b} \equiv \{b_{n,\boldsymbol{R}}\}$. $\mathbf{I} = [\delta_{n'n}\delta_{\boldsymbol{R}'\boldsymbol{R}}]$ is the identity matrix, where δ_{nm} is the kroneker delta. Elements of $\mathbf{A}$ are defined as

$$\mathbf{A}_{n',\boldsymbol{R}',n,\boldsymbol{R}} \equiv \frac{\Omega}{(2\pi)^3} \cdot \int_{\mathrm{BZ}} d\boldsymbol{k} e^{i\mathbf{k}\cdot(\boldsymbol{R}'-\boldsymbol{R})} \sum_m \left[\mathbf{U}^{(\boldsymbol{k})}_{n,m}\right] \omega^2_m(\boldsymbol{k}) \left[\mathbf{U}^{\dagger(\boldsymbol{k})}_{m,n'}\right]. \quad (8)$$

The permeability defect matrix $\mathbf{B}$ describes the coupling of the Wannier coefficients due to the magnetic defects and

$$\mathbf{B}_{n'',\boldsymbol{R}'',n,\boldsymbol{R}} \equiv \int_{\mathbb{R}} dr \nabla \times \boldsymbol{W}^{\dagger}_{n,\boldsymbol{R}} \underline{\eta}^{-1}_{\Delta}(\boldsymbol{r}) \nabla \times \boldsymbol{W}_{n'',\boldsymbol{R}''}. \quad (9)$$

The permittivity defect matrix $\mathbf{D}$ describes the coupling of the Wannier coefficients due to the dielectric defects and

$$\mathbf{D}_{n'',\boldsymbol{R}'',n,\boldsymbol{R}} \equiv \int_{\mathbb{R}} d\boldsymbol{r} \boldsymbol{W}^{\dagger}_{n'',\boldsymbol{R}''} \underline{\varepsilon}_{\Delta}(\boldsymbol{r}) \boldsymbol{W}_{n,\boldsymbol{R}}. \quad (10)$$

If we denote the number of lattice sites used in the expansion as $N_{\boldsymbol{R}}$ and the number of bands as N_n, then the number of elements in the vector $\mathbf{b}$ is $N_n N_{\boldsymbol{R}}$. The matrices $\mathbf{A}, \mathbf{B}$, and $\mathbf{D}$ have the same dimension of $N_n N_{\boldsymbol{R}} \times N_n N_{\boldsymbol{R}}$.

The efficiency of our design methods partly relies on the efficiency of the maximally localized Wannier basis expansion. First, because the Wannier functions are transformations of the Bloch waves, they contain information about the underlying crystal. As a result only a few Wannier basis functions per lattice site are needed to represent the field (i.e., the number of elements in the vector $\mathbf{b}$ is much less than the number of elements in a plane wave basis decomposition). Second, because the Wannier functions are highly localized, defects induce nonnegligible interactions only among Wannier functions centered on neighboring lattice sites [(9), (10)]. Therefore, due to the localization of the Wannier functions, the matrices $\mathbf{B}$ and $\mathbf{D}$ are sparse. Due to the complex exponential term, $\mathbf{A}$ is also sparse. All three matrices are banded (i.e., elements of the matrices quickly decay to zero away from the diagonal).

Equation (7) is very general; under most circumstances it can be further simplified. For example, when there are no magnetic perturbations, we can write (7) as

$$[\mathbf{I} + \mathbf{D}]\mathbf{b} = \beta \mathbf{A}\mathbf{b}, \quad \beta \equiv \omega^{-2}. \quad (11)$$

The matrix $\mathbf{A}$ is invertible since it is positive definite [10]. As a result, (11) can be solved as an eigenvalue equation for the modes and frequencies supported by a PC structure.

B. Linear Superposition of the Defects and Translation Property of Perturbation Matrices

An important property of the permittivity defect matrix $\mathbf{D}$ is that it can be decomposed into contributions from different defects. If we can decompose the defect $\underline{\varepsilon}_{\Delta}(\boldsymbol{r})$ into

$$\underline{\varepsilon}_{\Delta}(\boldsymbol{r}) = \sum_{\boldsymbol{i}} \underline{\varepsilon}_{\Delta,i}(\boldsymbol{r}) \quad (12)$$

it is straightforward to show from (10) that $\mathbf{D} = \Sigma_i \mathbf{D}_{\boldsymbol{i}}$, with $\mathbf{D}_{\boldsymbol{i}}$ defined by (10) with $\underline{\varepsilon}_{\Delta,\boldsymbol{i}}(\boldsymbol{r})$ in place of $\underline{\varepsilon}_{\Delta}(\boldsymbol{r})$. This is true even when the nonzero regions of the defect functions $\underline{\varepsilon}_{\Delta,\boldsymbol{i}}(\boldsymbol{r})$ are overlapping.

As an important special case, assume we can decompose the defect into contributions from each lattice site as $\underline{\varepsilon}_{\Delta}(\boldsymbol{r}) = \Sigma_{\mathbf{R}} \underline{\varepsilon}_{\Delta,\boldsymbol{R}}(\boldsymbol{r})$, where $\underline{\varepsilon}_{\Delta,\boldsymbol{R}}(\boldsymbol{r})$ is the contribution from lattice site $\boldsymbol{R}$. Furthermore assume the defects are the same, i.e., $\underline{\varepsilon}_{\Delta,\boldsymbol{R}}(\boldsymbol{r}-\boldsymbol{S}) = \underline{\varepsilon}_{\Delta,\boldsymbol{R}+\boldsymbol{S}}(\boldsymbol{r})$. Using the definition of Wannier functions, it is straightforward to show that $(\mathbf{D}_{\boldsymbol{R}})_{m',\boldsymbol{r}'-\boldsymbol{S},m,\boldsymbol{r}-\boldsymbol{S}} = (\mathbf{D}_{\boldsymbol{R}+\boldsymbol{S}})_{m',\boldsymbol{r}',m,\boldsymbol{r}}$, (i.e., $\mathbf{D}_{\boldsymbol{R}+\boldsymbol{S}}$ is a simple shift of $\mathbf{D}_{\boldsymbol{R}}$). This translation property of the perturbation matrix can greatly simplify the calculation of the defect matrix $\mathbf{D}$, which in turn can speed up sensitivity analysis and device optimization.

The situation is more complicated with the permeability perturbation matrix $\mathbf{B}$. We can decompose the defect $\underline{\mu}_{\Delta}(\boldsymbol{r})$ into $\underline{\mu}_{\Delta}(\boldsymbol{r}) = \Sigma_{\boldsymbol{i}} \underline{\mu}_{\Delta,\boldsymbol{i}}(\boldsymbol{r})$. The term that $\mathbf{B}$ relies on in (9) is in the form

$$\underline{\eta}^{-1}_{\Delta}(\boldsymbol{r}) = \left[\underline{\mu}_p(\boldsymbol{r}) \left(\sum_i \underline{\mu}_{\Delta,\boldsymbol{i}}(\boldsymbol{r})\right)^{-1} \underline{\mu}_p(\boldsymbol{r}) + \underline{\mu}_p(\boldsymbol{r})\right]^{-1}.$$

In order to write $\mathbf{B}$ as a sum, the above expression needs to be broken into a sum, which in general cannot be done. In a couple

of cases decomposition is possible. First, if there are no dielectric defects but only magnetic defects, then using the duality of the Maxwell's equations, the permeability perturbation matrix can be decomposed. Second, if $\underline{\mu}_{\Delta,i}(\boldsymbol{r})$ are disjoint in their nonzero regions, then $\underline{\eta}_{\Delta}^{-1}(\boldsymbol{r})$ can be composed and written as

$$\underline{\eta}_{\Delta}^{-1}(\boldsymbol{r}) = \sum_i [\underline{\mu}_p(\boldsymbol{r})(\underline{\mu}_{\Delta,\boldsymbol{i}}(\boldsymbol{r}))^{-1}\underline{\mu}_p(\boldsymbol{r}) + \underline{\mu}_p(\boldsymbol{r})]^{-1}.$$

If we just need to analyze an existing design, then we have the choice of breaking $\underline{\mu}_{\Delta}$ into spatially disjoint contributions. If we want to optimize a structure by changing an existing device, however, we may need to treat the change as an additional defect contribution. In that case, the additional defect may overlap with the existing defect, and we will not be able to perform the decomposition. Modifications to the permeability function cannot in general be treated as simple additive contributions to the permeability perturbation matrix $\mathbf{B}$. In the rest of this paper we will perform optimization and sensitivity analysis for dielectric constant perturbations only (though the original device may contain magnetic materials). If we want to optimize a structure by modifying solely the permeability function, we can use the duality of Maxwell's equations to convert the problem to an equivalent permittivity optimization problem. Efficient optimization involving concurrent permittivity function and permeability function changes remains a topic for future research.

III. Systematic Device Design Using Low Rank Adjustments of Matrix Inverse

The unique algebraic structure of the Wannier function basis enables extremely fast analysis of PC structures, particularly multiple structures that differ little from each other. Leveraging on this property, we can systemically design novel devices with complex prescribed functionalities by combining Wannier basis analysis with efficient optimization techniques to search through tens of thousands of possible designs.

A. Wannier Equations for Input/Output-Type Devices

Consider transmission-type devices, where PC waveguides are the ports that lead to a central defect region. Equation (7) can be rewritten in way such that it only deals with Wannier coefficients for lattices sites close to the central defect region (e.g., the boxed regions in Fig. 1.). Our formulation for input/output-type devices closely follows the formulation given by Busch [10]. We will highlight the structure of the equation that will be useful in the optimization process.

Without loss of generality, assume, for example, that the structure has two waveguide ports, where port 1 is a single mode waveguide and port 2 is a two mode waveguide. Assume the input excitation is in the form of the mode of waveguide 1. The waveguide regions defined in Fig. 1 are far enough from the central defect region such that the only nonzero fields are the propagating waveguide modes. A finite length vector of Wannier coefficients, $\mathbf{b}$, describes the field in the device. We can expand $\mathbf{b}$ in the waveguide regions by the normalized traveling waveguide modes. Let $\mathbf{g}_{ik}^{\pm}$ be the vector of Wannier

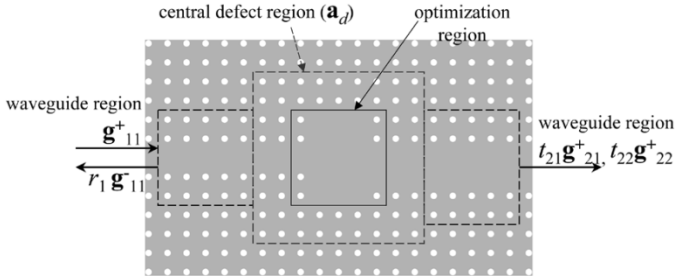

Fig. 1. White circles define the PC structure. Each box outlines the lattices sites associated with each Wannier coefficient vector. The regions are large enough so that there is negligible field outside the boxed regions except along the waveguide. The overlap between the waveguide regions and the evanescent field regions is needed to solve for the transmission and reflection coefficients.

coefficients describing mode k for waveguide i traveling to the right/left. We can write $\mathbf{b}$ as

$$\begin{aligned}\mathbf{b} &= \begin{bmatrix}\mathbf{g}_{11}^- & \mathbf{g}_{21}^+ & \mathbf{g}_{22}^+ & \mathbf{I}\end{bmatrix}\begin{bmatrix} r_1 \\ t_{21} \\ t_{22} \\ \mathbf{b}_d\end{bmatrix} + \mathbf{g}_{11}^+ \\ &\equiv \mathbf{C}\mathbf{x} + \mathbf{z}. \end{aligned} \tag{13}$$

In (13), r_1, t_{21}, and t_{22} are the reflection and transmission coefficients for the respective waveguide modes, and $\mathbf{b}_d$ is a vector of Wannier coefficients for lattice sites in the central defect region. By the notation $[\mathbf{a}\ \mathbf{b}\ \mathbf{c}\ \mathbf{M}]$, where $\mathbf{a}, \mathbf{b}$, and $\mathbf{c}$ are vectors and $\mathbf{M}$ is a matrix, we mean a matrix with the vectors $\mathbf{a}, \mathbf{b}$, and $\mathbf{c}$ as additional columns added to the left of the matrix $\mathbf{M}$. In (13), we defined $\mathbf{C} \equiv [\mathbf{g}_{11}^-\ \mathbf{g}_{21}^+\ \mathbf{g}_{22}^+\ \mathbf{I}], \mathbf{x} \equiv [r_1^T\ t_{21}^T\ t_{22}^T\ \mathbf{b}_d^T]^T$, and $\mathbf{z} \equiv \mathbf{g}_{11}^+$. The matrix $\mathbf{C}$ has more columns than rows. It is important to note that the vector $\mathbf{b}$ contains the Wannier coefficients for both the waveguide regions and the central defect region. Therefore, in (13), $\mathbf{g}_{ik}^{+/-}$ and $\mathbf{b}_d$ are padded with zeros of appropriate lengths.

We can now write (7) as

$$[(\mathbf{I} - \omega^{-2}\mathbf{A}) + \mathbf{D} - \omega^{-2}\mathbf{B}][\mathbf{C}\mathbf{x} + \mathbf{z}] = 0 \tag{14}$$

where $\mathbf{A}, \mathbf{D}$, and $\mathbf{B}$ are now truncated to have the dimension of the length of vector $\mathbf{x}$ (number of unknowns) times the length of vector $\mathbf{b}$ (number of Wannier coefficients in the central defect and the waveguide regions).

Now if we define

$$\begin{aligned}\mathbf{F} &\equiv [(\mathbf{I} - \omega^{-2}\mathbf{A}) + \mathbf{D} - \omega^{-2}\mathbf{B}]\mathbf{C} \\ \mathbf{y} &\equiv -[(\mathbf{I} - \omega^{-2}\mathbf{A}) + \mathbf{D} - \omega^{-2}\mathbf{B}]\mathbf{z}\end{aligned} \tag{15}$$

we get a matrix equation for the transmission-type devices

$$\mathbf{F}\mathbf{x} = \mathbf{y}. \tag{16}$$

The vector $\mathbf{y}$ describes the input excitation, and the system matrix $\mathbf{F}$ links the input excitation to the system state vector $\mathbf{x}$. The vector $\mathbf{x}$, describing the system state, contains both the Wannier coefficients for the central defect region and the amplitudes of the waveguide modes for the waveguide regions. Therefore, by solving (16), we fully characterize the device. For devices with as many as hundreds of lattice sites, $\mathbf{F}$ is small enough to be inverted in reasonable time on modest personal computing

hardware. It is extremely computationally expensive, however, to repeat the inverse calculation in the iterative loop of an optimization procedure. We will now develop a method to make design optimization computationally feasible.

B. Optimization

We start with an initial guess of the device design and form an initial system matrix $\mathbf{F}$. The transmission/reflection coefficients can then be found with (16) by finding $\mathbf{F}^{-1}$. Next we will modify the dielectric constant distribution to try to improve the transmission characteristic. In our algorithm, we assume there is very little information to guide us in the initial design. If the initial design is very far from the optimum then a local optimum found by gradient methods is not meaningful. In this case, a heuristic global search algorithm, such as simulated annealing, is more appropriate than gradient methods. This also restricts the allowable modifications to the dielectric constant distributions to a discrete set. As we will show by an example, if we work with a large number of unit cells, restricting allowable modifications to a discrete set still allows us to satisfy the transmission/reflection tolerances.

Without loss of generality, we will optimize the dielectric constant distribution of lattice sites in the optimization region (see Fig. 1). We assume each lattice site takes on one of the two allowed dielectric constant distributions (e.g., presence or absence of a dielectric rod at a lattice site). Generalization to a larger set of allowed distributions is straightforward. We will use a simulated annealing algorithm to choose the modification at each step. Let the allowed modification to the lattice site $\mathbf{R}$ be given by $\underline{\varepsilon}_{\delta,\boldsymbol{R}}$. A modification changes the dielectric constant distribution to $\underline{\varepsilon}_p(\boldsymbol{r}) + \underline{\varepsilon}_\triangle(\boldsymbol{r}) + \underline{\varepsilon}_{\delta,\boldsymbol{R}}(\boldsymbol{r})$. As we pointed out in Section II.B, the perturbation matrix, $\mathbf{D}_{\delta,\mathbf{R}}$, associated with the modification only needs to be calculated once for one lattice site. The perturbation matrices for all other lattice sites are simple translations of the one found. Equation (14) now becomes

$$[(\mathbf{I} - \omega^{-2}\mathbf{A}) + (\mathbf{D} + \mathbf{D}_{\delta,\mathbf{R}}) - \omega^{-2}\mathbf{B}][\mathbf{C}\mathbf{x} + \mathbf{z}] = 0$$

where $\mathbf{D}_{\delta,\mathbf{R}}$ is defined by (10), but with $\underline{\varepsilon}_{\delta,\boldsymbol{R}}(\boldsymbol{r})$ in place of $\underline{\varepsilon}_\triangle(\boldsymbol{r})$. This equation can be written as

$$\mathbf{F}\mathbf{x} - \mathbf{y} + \mathbf{D}_{\delta,\mathbf{R}}[\mathbf{C}\mathbf{x} + \mathbf{z}] = 0.$$

Since $\mathbf{D}_{\delta,\mathbf{R}}$ is only nonzero for a few lattice sites around the modified lattice site, the modification in the optimization region does not affect the system matrix in the waveguide regions. Therefore, $\mathbf{D}_{\delta,\mathbf{R}}\mathbf{C} = \mathbf{D}_{\delta,\mathbf{R}}$. For the same reason, $\mathbf{D}_{\delta,\mathbf{R}}\mathbf{z} = 0$. Therefore, the system equation for the modified device is simply

$$(\mathbf{F} + \mathbf{D}_{\delta,\mathbf{R}})\mathbf{x} = \mathbf{y}. \tag{17}$$

After modifying the structure, we can find the new transmission/reflection coefficients using (17). We can then iterate the tuning process until the tolerances on the transmission/reflection coefficients are satisfied.

The main cost of the optimization is solving (17) in each search step. Let k be the size of the system matrix $\mathbf{F}$. k is typically several thousand for devices made of several hundred lattice sites. In our method, we dramatically speed up the search process by taking advantage of a low rank matrix inverse update, made possible by the highly localized Wannier basis.

Because the Wannier functions are localized to a few unit cells, the $k \times k$ matrix $\mathbf{D}_{\delta,\mathbf{R}}$ is zero everywhere except for a small number of elements that couple the Wannier coefficients for the modified lattice site to the coefficients for the neighboring lattice sites. We can then write $\mathbf{D}_{\delta,\mathbf{R}}$ as the product of the nonzero region of $\mathbf{D}_{\delta,\mathbf{R}}$ (with dimensions smaller than $k \times k$) with two rectangular matrices. The rectangular matrices are slices of the identity matrix. Their function is to position the nonzero region at the correct location in $\mathbf{D}_{\delta,\mathbf{R}}$.

For example, if $k = 1000$, and $\mathbf{D}_{\delta,\mathbf{R}}$ is zero everywhere except in the block ranging from row 101 to 130 and column 101 to 130, we can then denote $\mathbf{E}$ as the sub-matrix in $\mathbf{D}_{\delta,\mathbf{R}}$ containing all of the nonzero elements, with dimension $l \times l, l = 30$. We then have

$$\mathbf{D}_{\delta,\mathbf{R}} = \mathbf{X}_\mathbf{R}\mathbf{E}\mathbf{Y}_\mathbf{R} \tag{18}$$

where $\mathbf{X}_\mathbf{R} = [\mathbf{0}_{\mathbf{R}1}\ \mathbf{I}\ \mathbf{0}_{\mathbf{R}2}]^T \in \mathbb{R}^{k\times l}, \mathbf{E} \in \mathbb{R}^{l\times l}$, and $\mathbf{Y}_\mathbf{R} = [\mathbf{0}_{\mathbf{R}1}\ \mathbf{I}\ \mathbf{0}_{\mathbf{R}2}] \in \mathbb{R}^{l\times k}$. The identity matrix $\mathbf{I}$ has the same dimension as $\mathbf{E}$. $\mathbf{0}_{\mathbf{R}1} \in \mathbb{R}^{100\times 30}$ and $\mathbf{0}_{\mathbf{R}2} \in \mathbb{R}^{870\times 30}$ are rectangular block matrices of all zeros.

The matrix $\mathbf{E}$ is typically not well conditioned, i.e., the many elements in $\mathbf{E}$ can be very small, particularly elements describing the coupling of Wannier functions several lattice sites apart. Therefore, we use a singular value decomposition to write

$$\mathbf{E} = \mathbf{V}\mathbf{H}\mathbf{W} \tag{19}$$

where $\mathbf{V} \in \mathbb{R}^{l\times j}, \mathbf{H} \in \mathbb{R}^{j\times j}$, and $\mathbf{W} \in \mathbb{R}^{j\times l}$. In the end, the rank of the update matrices $\mathbf{D}_{\delta,\mathbf{R}}$ is j, which is typically much less than 100.

Now, in order to find the new transmission coefficient for a possible modification, we need to solve (17). In our method, we dramatically speed up the inversion of $(\mathbf{F} + \mathbf{D}_{\delta,\mathbf{R}})$ by taking advantage of the low rank of $\mathbf{D}_{\delta,\mathbf{R}}$. We can find $(\mathbf{F} + \mathbf{D}_{\delta,\mathbf{R}})^{-1}$ using an expression for the inverse of a small rank adjustment [15], for which we provide a derivation in Appendix B.

$$(\mathbf{F} + \mathbf{D}_{\delta,\mathbf{R}})^{-1} = \mathbf{F}^{-1} - \mathbf{F}^{-1}\mathbf{X}\mathbf{V}(\mathbf{H}^{-1} + \mathbf{W}\mathbf{Y}\mathbf{F}^{-1}\mathbf{X}\mathbf{V})^{-1}\mathbf{W}\mathbf{Y}\mathbf{F}^{-1} \tag{20}$$

where $\mathbf{X}, \mathbf{Y}, \mathbf{V}, \mathbf{W}, \mathbf{H}$ are given in (19) and (18). Despite the longer form, (20) involves the inversion of two matrices of dimension $j \times j$, and uses $\mathbf{F}^{-1}$ that was already calculated for the initial design. j is typically less than 100, while the dimension of the system matrix $\mathbf{F}$ is k, which can be several thousand. Because a matrix inversion has a complexity of $\mathrm{O}(n^3)$, using (20) to find the inverse is at least three orders of magnitude faster than direct inversion. This speedup means that simulated annealing based heuristic search has become a computationally practical design method for PC devices.

The one time inversion of $\mathbf{F}^{-1}$ in the initial step is computationally expensive. Because the cost of computing $\mathbf{F}^{-1}$ scales cubically with the number of lattice sites, while FDTD simulation scales linearly, for large structures (with several hundred lattice sites), the inversion requires roughly the same

amount of time as a FDTD simulation. However, once $\mathbf{F}^{-1}$ is found, using the method presented, transmission for new designs can be found at least 1000× faster than rerunning FDTD simulations.

There is also a computational overhead for calculating $\mathbf{D}_{\delta,\mathbf{R}}$, or more specifically, $\mathbf{V}, \mathbf{W}, \mathbf{H}$. As we have shown in II.B, however, this computation only needs to be performed once for one type of perturbation to a unit cell. The computational cost is amortized over the analysis of applying the same perturbation to other unit cells, for any device constructed in the same PC.

IV. Sensitivity Analysis in Wannier Basis

Once we have found an acceptable design using a global search within a set of discrete modifications, we can fine-tune the device by using certain continuously tunable parameters of the dielectric constant distribution (e.g., index or radius of a rod for a PC unit cell). In this case, the sensitvity of the performance parameters with respect to small perturbations is useful for picking the fine-tuning steps.

We will now develop our WBG sensitivity analysis method as a separate topic, and tie it to the optimization procedure in the next section. The sensitivity analysis itself has additional applications such as evaluating the robustness of PC devices against perturbations.

A. Transmission Coefficient Sensitivity

We will again assume that each perturbation is restricted to the unit cell of a single lattice site, and occurs in the optimization region (see Fig. 1). The optimization algorithm in Section III-B can be used to treat both lossless and lossy defect structures in a lossless periodic system. Here, however for the sensitivity analysis, we assume the defect structure itself is lossless as well. Furthermore, we assume that the perturbation term is isotropic.

We employ an adjoint-variable method (AVM) to analyze the sensitivity. AVM was first applied to PC structures by Veronis [8] for the FDTD method. Here we will elaborate on its usage and additional advantages under the Wannier basis.

Assume γ parameterizes the small perturbation $\underline{\varepsilon}_{\delta,0}(\boldsymbol{r},\gamma)$ such that $\underline{\varepsilon}_{\delta,0}(r,0)=0$. $\mathbf{D}_{\delta,0}$ and $\mathbf{x}$ are then functions of γ. To find the sensitivity of the transmission coefficients w.r.t γ, we take the derivative of (17) w.r.t. γ and get

$$\frac{d}{d\gamma}[\mathbf{D}_{\delta,0}(\gamma)]\mathbf{x}(\gamma)+[\mathbf{F}+\mathbf{D}_{\delta,0}(\gamma)]\frac{d}{d\gamma}\mathbf{x}(\gamma)=0. \tag{21}$$

Rearranging and evaluating at $\gamma=0$, we get

$$\frac{d}{d\gamma}\mathbf{x}(\gamma)=-\mathbf{F}^{-1}\frac{d}{d\gamma}[\mathbf{D}_{\delta,0}(\gamma)]\mathbf{x}(\gamma). \tag{22}$$

Formally, one of the transmission/reflection coefficients is given by $t(\gamma)=\mathbf{e}^T\mathbf{x}(\gamma)$, where $\mathbf{e}^T$ is a unit vector in the form $[0\ \cdots\ 1\ \cdots\ 0]$. The sensitivity of t is then

$$\frac{d}{d\gamma}t(\gamma)=-\mathbf{e}^T\mathbf{F}^{-1}\frac{d}{d\gamma}[\mathbf{D}_{\delta,0}(\gamma)]\mathbf{x}(\gamma). \tag{23}$$

Following the AVM formulation, we define a vector $\bar{\mathbf{x}}\equiv[\mathbf{e}^T\mathbf{F}^{-1}]^\dagger$ that is a solution to the adjoint problem

$$[\mathbf{F}^\dagger]\bar{\mathbf{x}}=\mathbf{e}. \tag{24}$$

With the definition of $\mathbf{F}$ from (15) we have

$$\mathbf{F}^\dagger=\mathbf{C}^\dagger[(\mathbf{I}-\omega^{-2}\mathbf{A})+\mathbf{D}-\omega^{-2}\mathbf{B}]$$

where we have used the fact that $\mathbf{A},\mathbf{D}$, and $\mathbf{B}$ are Hermitian if the original structure is lossless. Equation (23) then takes the form

$$\frac{d}{d\gamma}t(\gamma)=-\bar{\mathbf{x}}^\dagger\frac{d}{d\gamma}[\mathbf{D}_{\delta,0}(\gamma)]\mathbf{x}(\gamma). \tag{25}$$

We obtained $\mathbf{F}^{-1}$ when solving the transmission of the nonperturbed structure, so $\mathbf{x}$ and $\bar{\mathbf{x}}$ can be found with simple multiplications. Due to the localization of the Wannier functions to a few neighboring unit cells, $\partial\mathbf{D}_{\delta,0}/\partial\gamma$ typically only has a few hundred nonzero elements. Multiplying a few matrices and vectors with a few hundred elements is a trivial computation for most modern personal computers. After we properly define and calculate $\partial\mathbf{D}_{\delta,0}/\partial\gamma$, we will be able to use (25) to find the gradient of one of the transmission coefficients with respect to γ with a simple multiplication.

We can evaluate $[\partial\mathbf{D}_{\delta,0}(\gamma)/\partial\gamma]_{n'',\boldsymbol{R}'',n,\boldsymbol{R}}$ as

$$\begin{aligned}
&\frac{\partial}{\partial\gamma}\int_{\mathbb{R}^3}dr\boldsymbol{W}^\dagger_{n'',\boldsymbol{R}''}(\boldsymbol{r})\underline{\varepsilon}_{\delta,0}(\boldsymbol{r},\gamma)\boldsymbol{W}_{n,\boldsymbol{R}}(\boldsymbol{r})\Big|_{\gamma=0}\\
&\quad=\int_{\mathbb{R}^3}dr\boldsymbol{W}^\dagger_{n'',\boldsymbol{R}''}(\boldsymbol{r})\frac{\partial}{\partial\gamma}\underline{\varepsilon}_{\delta,0}(\boldsymbol{r},\gamma)W_{n,\boldsymbol{R}}(\boldsymbol{r})\Big|_{\gamma=0}\\
&\quad=\int_{\mathbb{R}^3}dr\boldsymbol{W}^\dagger_{n'',R''}(\boldsymbol{r})\frac{\partial\underline{\varepsilon}(\boldsymbol{r},\gamma)}{\partial\gamma}W_{n,\boldsymbol{R}}(\boldsymbol{r})\Big|_{\gamma=0}
\end{aligned} \tag{26}$$

where switching integration and differentiation is justified because all the integrals converge uniformly. From line two to line three of (26), we used the fact that the change in the perturbation of the dielectric function is the same as the change in the overall dielectric function.

1) Dielectric Constant Scaling Perturbations: One type of perturbation where $\partial\mathbf{D}_{\delta,0}/\partial\gamma$ is easily defined is the local scaling of the dielectric constant distribution. For example, because of effects such as temperature changes or presence of electric fields, we could have a scaling of $\underline{\varepsilon}_{\Delta,\boldsymbol{R}}(\boldsymbol{r})$ at a lattice site $\boldsymbol{R}$. This perturbation can be written as $\gamma\underline{\varepsilon}_{\Delta,\boldsymbol{R}}(\boldsymbol{r})$, where γ parameterizes the perturbation. From (26), we have $\partial\mathbf{D}_{\delta,0}/\partial\gamma=\mathbf{D}_{\boldsymbol{R}}$, with $\mathbf{D}_{\boldsymbol{R}}$ defined in Section II.B. The sensitivity calculation using (25) then follows without any numerical difficulty.

2) Boundary Shift Perturbations: Another important type of perturbation is the shift in the dielectric boundary. In this case, however, the calculation of $\partial\mathbf{D}_{\delta,0}/\partial\gamma$ is less straightforward. Assume the unperturbed dielectric constant distribution $\underline{\varepsilon}_p(\boldsymbol{r})+\underline{\varepsilon}_\Delta(\boldsymbol{r})$ is piecewise constant, and the perturbation $\underline{\varepsilon}_{\delta,0}(\boldsymbol{r},\gamma)$ causes a shift of the boundary between the two materials. Because the derivative in the integral is only nonzero close

to the shifting material boundary, we only need to consider the integration over a small volume covering the boundary shift. For simplicity, consider the contribution to the integral by a small volume covering an infinitesimal area dA of the dielectric boundary. This contribution can be written as a one-dimensional (1-D) integral

$$dA \int dz \boldsymbol{W}^{\dagger}_{n'',\boldsymbol{R}''}(z) \frac{\partial \underline{\varepsilon}(z,\gamma)}{\partial \gamma} \boldsymbol{W}_{n,\boldsymbol{R}}(z)\bigg|_{\gamma=0} \tag{27}$$

where we have oriented the coordinate system such that z is normal to the dielectric boundary, and dA is the area of the dielectric boundary in the integration volume. We also shifted the z axis so that the dielectric boundary is at $z=0$ when $\gamma=0$. In the vicinity of the dielectric boundary, we can write the dielectric constant distribution as

$$\underline{\varepsilon}(z) = \underline{\varepsilon}_a + (\underline{\varepsilon}_b - \underline{\varepsilon}_a)\Theta(z-\gamma) \tag{28}$$

where $\underline{\varepsilon}_a$ and $\underline{\varepsilon}_b$ are the dielectric tensors on each side of boundary. If we try to evaluate the derivative directly, we get

$$(\underline{\varepsilon}_a - \underline{\varepsilon}_b) \int dz \boldsymbol{W}^{\dagger}_{n'',\boldsymbol{R}''}(z)\delta(z)\boldsymbol{W}_{n,\boldsymbol{R}}(z). \tag{29}$$

We will now show that this expression is ill defined. Substituting (29) back into (25), we get the following expression for the sensitivity:

$$\begin{aligned}\frac{d}{d\gamma}t(\gamma) &= -(\underline{\varepsilon}_a - \underline{\varepsilon}_b)\int dz \bar{\boldsymbol{E}}^{\dagger}(z)\,\delta(z)\boldsymbol{E}(z) \\ &= -(\underline{\varepsilon}_a - \underline{\varepsilon}_b)\bar{\boldsymbol{E}}^{\dagger}(0)\boldsymbol{E}(0)\end{aligned} \tag{30}$$

where we have used the fact that the perturbation is in the central defect region so that $\Sigma(\mathbf{x})_{n,\boldsymbol{R}}\boldsymbol{W}_{n,\boldsymbol{R}} = \boldsymbol{E}$, and we have defined $\bar{\boldsymbol{E}} \equiv \Sigma(\bar{\mathbf{x}})_{n'',\boldsymbol{R}''}W_{n'',\boldsymbol{R}''}$. Now, because of the material boundary, the normal components of $\bar{\boldsymbol{E}}$ and $\boldsymbol{E}$ are discontinuous at $z=0$, and the value of (30) is ill defined.

The source of this dilemma is elaborated by Johnson [16]. The problem is that an infinitesimal boundary shift introduces a finite change in the dielectric constant distribution, which means there is a finite change to the E-field. When we are taking the derivative, however, we assume infinitesimal change in $\bar{\boldsymbol{E}}$ and $\boldsymbol{E}$ when γ changes by an infinitesimal amount.

To find a physically meaningful quantity for (27), we can treat it as the limit of a structure with smoothed dielectric constant distribution. With a appropriate smoothing function and taking the limit using a procedure similar to Johnson [16], we can resolve the ambiguity due to the field discontinuity. In the isotropic case, the resulting equation for $\partial \mathbf{D}_{\delta 0}/\partial\gamma$ is

$$\begin{aligned}&\frac{\partial (\mathbf{D}_{\delta 0})_{n'',\boldsymbol{R}'',n,\boldsymbol{R}}}{\partial \gamma} \\ &= \oint_{h(0,\boldsymbol{r})} dA(\varepsilon_a - \varepsilon_b)\boldsymbol{W}^{\dagger}_{\|,n'',\boldsymbol{R}''}(\boldsymbol{r})\boldsymbol{W}_{\|,n,\boldsymbol{R}}(\boldsymbol{r}) \\ &\quad - \oint_{h(0,\boldsymbol{r})} dA\left(\varepsilon_a^{-1} - \varepsilon_b^{-1}\right) \\ &\quad \times \varepsilon(\boldsymbol{r})^2 \boldsymbol{W}^{\dagger}_{\perp,n'',\boldsymbol{R}''}(\boldsymbol{r})\boldsymbol{W}_{\perp,n,\boldsymbol{R}}(\boldsymbol{r})\end{aligned} \tag{31}$$

where $\boldsymbol{W}_{\|,n,\boldsymbol{R}}(\boldsymbol{r})$ is the component of the Wannier function tangential to the material boundary, $\boldsymbol{W}_{\perp,n,\boldsymbol{R}}(\boldsymbol{r})$ is the normal component, and the surface integral is along the material boundary $h(0,\boldsymbol{r})$. ε_a and ε_b are the dielectric constants on the opposite sides of the dielectric discontinuity. We can check that the ambiguity is indeed resolved. Substituting (31) back into (25), we get the following expression for the sensitivity:

$$\begin{aligned}\frac{d}{d\gamma}t(\gamma) &= \oint_{h(0,\boldsymbol{r})} dA(\varepsilon_a - \varepsilon_b)\bar{\boldsymbol{E}}^{\dagger}_{\|}(\boldsymbol{r})\bar{\boldsymbol{E}}_{\|}(\boldsymbol{r}) \\ &\quad - \oint_{h(0,\boldsymbol{r})} dA\left(\varepsilon_a^{-1} - \varepsilon_b^{-1}\right)\varepsilon(\boldsymbol{r})^2 \bar{\boldsymbol{E}}^{\dagger}_{\perp}(\boldsymbol{r})\bar{\boldsymbol{E}}_{\perp}(\boldsymbol{r}).\end{aligned} \tag{32}$$

The tangential component of the E-field and the permittivity times the normal component of the E-field are both continuous across the boundary, so (32) gives the same value regardless of from which side of the boundary we evaluate the integral. Therefore, $\partial \mathbf{D}_{\delta,0}/\partial\gamma$, as defined by (31), will give the same sensitivity regardless of on which side the boundary we evaluate (31).

3) Advantages of WBG: After we determine the perturbation matrix $\partial \mathbf{D}_{\delta 0}/\partial\gamma$ for one specific unit cell, applying the same perturbation to other unit cells, or multiples of them, is computationally trivial. Following the argument in Section II-B, if the dielectric constant distribution changes by $\Sigma_{\boldsymbol{R}}[\underline{\varepsilon}_{\delta,\boldsymbol{R}}(\boldsymbol{r},\gamma)]$, it is straightforward to show that the sensitivity can be evaluated as

$$\frac{d}{d\gamma}t(\gamma) = -\bar{\mathbf{x}}^{\dagger}\sum_{\boldsymbol{T}} \frac{d\mathbf{D}_{\delta,\mathbf{T}}}{d\gamma}\mathbf{x}(\gamma) \tag{33}$$

where

$$(\partial \mathbf{D}_{\delta,\mathbf{T}}/\partial\gamma)_{n\mathbf{R},m\mathbf{S}} = (\partial \mathbf{D}_{\delta,0}/\partial\gamma)_{n(\mathbf{R}-\boldsymbol{T}),m(\mathbf{S}-\boldsymbol{T})}. \tag{34}$$

Matrix shift is a trivial operation. Therefore, after a one-time calculation of $\partial \mathbf{D}_{\delta 0}/\partial\gamma$, we can use (33) to map out the sensitivity to the perturbation of each and every unit cell, as well as coherent effects caused by simultaneous perturbation of multiple unit cells. All this can be done in a matter of seconds on modest personal computing hardware.

Sensitivity analysis in the Wannier basis can greatly reduce the required resolution on the computational grid. Actual numerical implementation of any sensitivity analysis method involves approximating continuous functions by discretization. For small shifts in the material boundary, direct finite difference using FDTD or PWM needs high-resolution computational grids in order to resolve the perturbation. In our method, the integral in (31) is approximated by a discrete sum over a discrete spatial grid. Assume the Wannier functions are found on a computational grid too coarse to resolve the boundary shift. Because both $\varepsilon(\boldsymbol{r})\boldsymbol{W}_{\perp,n,\boldsymbol{R}}(\boldsymbol{r})$ and $\boldsymbol{W}_{\|,n,\boldsymbol{R}}(\boldsymbol{r})$ are continuous and vary significantly only over distances comparable to the wavelength, simple interpolation of the Wannier functions to a higher resolution grid can increase the accuracy of (31).

4) Eigenfrequency Sensitivity: Under the Wannier function expansion, we can also calculate the sensitivity of resonator eigenfrequencies to perturbations. Again we first consider a perturbation to one unit cell in the vicinity of the resonator cavity. If γ parameterizes the perturbation $\underline{\varepsilon}_{\delta,0}(\boldsymbol{r},\gamma)$, then the master equation for the eigenfrequency, (11), becomes

$$(\mathbf{I} + \mathbf{D} + \mathbf{D}_{\delta,0}(\gamma))\mathbf{b} = \beta(\gamma)(\mathbf{A}+\mathbf{B})\mathbf{b}. \tag{35}$$

We can directly solve (35) as a generalized eigenvalue equation for the new resonator eigenmodes. If $\beta(\gamma)$ is an nondegenerate generalized eigenvalue, we have shown in Appendix C that the sensitivity of $\beta(\gamma)$ is given by

$$\frac{d\beta(\gamma)}{d\gamma} = \frac{\mathbf{w}^\dagger(\gamma)(d\mathbf{D}_{\delta,0}/d\gamma)\mathbf{b}(\gamma)}{\mathbf{w}^\dagger(\gamma)(\mathbf{A}+\mathbf{B})\mathbf{b}(\gamma)} \tag{36}$$

where $\mathbf{w}$ is a left eigenvector associated with $\beta(\gamma)$ such that

$$\mathbf{w}^\dagger(\mathbf{I}+\mathbf{D}+\mathbf{D}_{\delta,0}(\gamma)) = \beta(\gamma)\mathbf{w}^\dagger(\mathbf{A}+\mathbf{B}). \tag{37}$$

If we assume that the structure before perturbation is lossless, then $\mathbf{w} = \mathbf{b}$. Using the definition of $\partial\mathbf{D}_{\delta,0}/\partial\gamma$ from (26), and the fact that $\Sigma b_{n,\boldsymbol{R}}\boldsymbol{W}_{n,\boldsymbol{R}} = \boldsymbol{E}$, we get

$$\frac{d\beta(\gamma)}{d\gamma} = \frac{\int\limits_{\mathbb{R}^3} d\boldsymbol{r}\boldsymbol{E}^\dagger(\boldsymbol{r})\frac{\partial\varepsilon(\boldsymbol{r},\gamma)}{\partial\gamma}\boldsymbol{E}(\boldsymbol{r})}{\mathbf{b}^\dagger(\gamma)(\mathbf{A}+\mathbf{B})\mathbf{b}(\gamma)}. \tag{38}$$

This is the same result as derived from perturbation theory [16]. However, in contrast to (38), (36) is a computationally trivial matrix multiplication, involving $\partial\mathbf{D}_{\delta,0}/\partial\gamma$ and a few parameters that are independent of the perturbation and easily obtained when we calculated the eigenfrequency using (11). All the advantages from calculating $\partial\mathbf{D}_{\delta,0}/\partial\gamma$ first and reusing it, mentioned in the previous section, still apply here. As a result this method possesses significant speed savings over doing field integrals every time using (38). We will refer to both (36) and (25) as the WBG method for sensitivity analysis.

For sensitivity analysis involving shifts in the dielectric boundary, we again use (31) to calculate $\partial\mathbf{D}_{\delta,0}/\partial\gamma$. Using (36) and the fact that $\Sigma b_{n,\boldsymbol{R}}\boldsymbol{W}_{n,\boldsymbol{R}} = \boldsymbol{E}$, it is straightforward to show that this method of finding $\partial\mathbf{D}_{\delta,0}/\partial\gamma$ resolves any ambiguity due to field discontinuities.

V. Systematic Device Design With Wannier Basis Local Optimization

We envision a typical design process where we use either the Wannier basis discrete global search or some other means to obtain a device design that is close to meeting the design specification. Normally, we can improve the device performance by fine-tuning parameters such as the dielectric constant or the dimension of a geometrical feature of each unit cell in the optimization region. In this section we present the design algorithm that fine tunes PC device designs systematically in computationally practical time. The algorithm uses the WBG sensitivity analysis and the small rank adjustment discrete update [(20)] as building blocks, applies the two blocks in a repeated leapfrog fashion, and efficiently reuses intermediate calculations from one block to the next.

We start by calculating gradient vectors $dt_1/d\vec{\gamma},\ldots,dt_m/d\vec{\gamma}$, where t_m represents the transmission on the desired output for output channel m, and $\vec{\gamma} = \{\gamma_{\vec{\boldsymbol{R}}}, \vec{\boldsymbol{R}} = \boldsymbol{R}_1,\ldots,\boldsymbol{R}_N\}$ parameterizes the fine-tuning for each of the N unit cells. To make the fine-tuning computationally efficient, we fine-tune the same parameter for each unit cell. An element in the vector for the rod at $\boldsymbol{R}_i$ is calculated using (23). Because the same type of perturbation is applied to all N unit cells, we only need to calculate the matrix $\partial\mathbf{D}_{\delta,0}/\partial\gamma$ for a single unit cell, and the remaining matrices are related to $\partial\mathbf{D}_{\delta,0}/\partial\gamma$ by trivial shifts as described in Section II.B. For devices of typical sizes, calculating the gradient vectors with a total of $\sim$100 elements only takes a few minutes on a Pentium III computer.

To fine-tune the design for better performance, we try to minimize the cost function

$$\sum_{i=1}^{m}(t_i - \hat{t}_i)^2$$

where $\hat{t}_i$ is the desired transmission for output channel i. The gradient of this cost function with respect to the fine-tuning parameters can be found using the transmission gradients, found in the first step, and the chain rule. Of course, there could be more complicated design specifications, such as controlling the phase of the transmission, or controlling the field strength on specific locations of the device. Because the Wannier basis analysis is a rigorous method for calculating the field, the gradients of all such parameters w.r.t. fine-tuning parameters can be obtained through WBG sensitivity analysis.

Using the WBG method to find the gradient efficiently, we can then apply any gradient-based local optimization algorithm to search for a local optimal in the design. Such methods include steepest descent and conjugate gradients .[17]. In each iteration, after the optimization algorithm chooses a direction and distance to go in the design space, we need to evaluate the performance of the new trial design. The small rank adjustment method described in Section III-B is used again. The modification to the device given by the local optimization algorithm can be treated as a small rank adjustment to the system, and new transmission coefficients can be found very quickly using (20). For typical device sizes, it only takes a few minutes to find the new transmission coefficients on a Pentium III computer.

From (20), we also obtain the inverse of the new system matrix. For the next iteration in the optimization, the new inverse is then used in (23) to find the gradient for the modified structure. After the gradient is found, the process repeats until we have found the local design optimum. As we can see, this process is very efficient because the update and gradient calculation of the local optimization can be both done in the Wannier basis, allowing the gradient calculation to benefit from the intermediate result of the update calculation.

The fine-tuning involves modifying the structure in iterations. The matrix $\partial\mathbf{D}_{\delta,0}/\partial\gamma$ only has to be calculated once if we only scale the dielectric constant of a feature in each unit cell. Tuning the geometry of the feature, however, needs to be done discretely, because the perturbation matrix $\partial\mathbf{D}_{\delta,0}/\partial\gamma$ for geometry change may not scale linearly with the change. To solve this problem, we can discretize the range of geometrical variation into a discrete set. For example, if we are changing the rod radius in a PC of high index rods, we can approximate the continuous radius change by a set of discrete values. Practically speaking, a set with 50 radius change steps would be more than sufficient, because the resolution would exceed today's fabrication error tolerances, and the step size would be much smaller than a wavelength. We would then proceed to calculate 50 perturbation matrices $\mathbf{D}_{\delta,0}$ and their derivatives $\partial\mathbf{D}_{\delta,0}/\partial\gamma$ once for all, one for each step in the rod radius increase. In each step

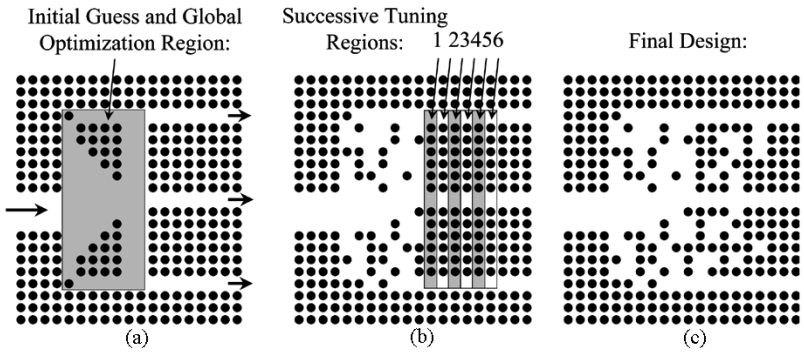

Fig. 2. (a) Initial guess at the mode separator structure. The PC parameters are given in the text. Arrows shows the input and output ports. The dashed rectangle shows the optimization region of the structure that is altered in the search process. (b) Device before enlargement. The numbered boxes represent the regions and the order to which the optimization is applied. The existing device region is not changed in the optimization. (c) Final device after increasing device size.

of the optimization, the perturbation matrices will be chosen based on the current value of the fine-tuning parameters. The desired modification would be approximated using the allowable radii in the discretized set, and the procedure would be repeated. Additional constraints, such as minimum radius that can be fabricated, can be included in the design process by using a sequential quadratic programming optimization method [18] rather than conjugate gradient.

The number of steps needed to converge to the local optimum depends on the initial design, i.e., the design obtained using the discrete Wannier basis global search. The number of steps also depends on the number of fine-tuning parameters and the optimization algorithm used. For the numerical examples in the next section, the number of steps necessary is typically in the range of hundreds.

Finally, we must stress that the small rank adjustment is vital to enabling a local optimization algorithm. Until now, perturbative methods have been the only computationally practically way for repeatedly calculating the device characteristics when many design parameters are perturbed. However, a local optimization process can take hundreds or thousands of steps to converge. The cumulative error of a perturbative method for calculating performance numbers can render the local optimization useless. Our low rank update method, however, is an exact process for updating the performance figure in each local optimization step, with a computational complexity comparable to perturbative methods. This is the key to enabling a viable local optimization algorithm for PC device design.

VI. Numerical Example

We demonstrate our small rank adjustment design method using a mode separator design example. We wish to design a device that separates three guiding modes of a multimode waveguide around an operating wavelength of 1503 nm. Previous mode separator designs either use adiabatic mode transformation [19], which makes the devices very long, or they rely on the symmetry of the modes [20], which limits the separation to odd and even modes. Our design does not have either of these shortcomings. We start with a 2-D PC made of high index cylinders ($n = 3.4, \text{rod radius} = 0.18a, a = \text{lattice constant}$) in air. The initial guess for the design is shown in Fig. 2(a). The input waveguide made of three rows of missing rods supports three

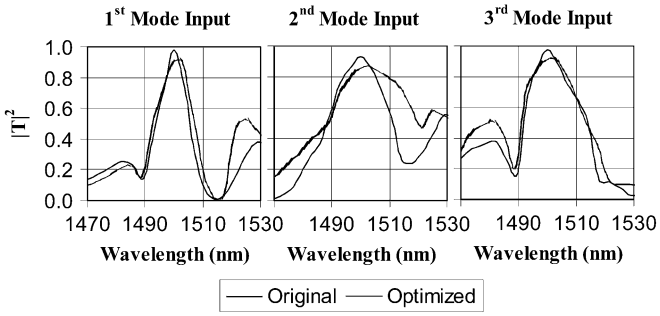

Fig. 3. Power transmission spectra at the intended output ports for 3 input modes. The original and the optimized spectra correspond to structures shown in Fig. 2(a) and (b) respectively. The peak transmission is improved in the optimized structure without significant degradation to the bandwidth.

modes. The three output single mode waveguides are made of single rows of missing rods. The final design will take the three modes of the input guide and separate them into the three output waveguides. The initial guess shown is quite arbitrary, however, and the initial structure does not act like a mode separator at all.

Next we search for a better design by removing or adding rods to the optimization region outlined in Fig. 2(a). Using the small rank adjustment global optimization described in Section III-B, we obtain the mode separator design shown in Fig. 2(b), with transfer functions shown by the dashed curves in Fig. 3. For all three input modes, the contrast ratio of the intended output to the unwanted output is greater than 15 dB. The contrast ratio between the intended output and the reflection is greater than 10 dB. The device size is 13×21 lattice constants. For 1.5-μm operation, this means a device size of $8.2 \times 13.3\,\mu$m. In comparison, mode filters using multimode interference couplers are $>100\ \mu$m in length [20]. It should be noted that the device size we quote is the area with nonnegligible field, not just the area with defects. This is the most compact mode separator/converter known to the authors. We now show different Wannier finetuning methods for greatly improving the performance of this design.

A. Fine-Tuning by Trading Off Device Size for Performance

We see from Fig. 3 that the peak transmission for the original design is $\sim$90%. We achieved this in a binary design space with 105 rods (removal or addition of each rod). We could improve the performance further by solving several much smaller optimization problems at the expense of enlarging the device area.

More specifically, in the first optimization step, we will remove or add the high index rods forming the PC, in the boxed region 1 shown in Fig. 2(a). We use (20) to calculate the new transmission/reflection. In the second step, we optimize the rods in box 2. Repeating the process, the device performance is improved by successively stacking layers of perturbation to the output of the device. The performance measure is the sum of the square of all unwanted reflections and transmissions for all three input modes.

In the Wannier basis global optimization to obtain the design in Fig. 2(b), the search was done using simulated annealing. A systematic search was impractical because there were 2^{105} possible designs. In the six device enlargement steps, however, we only consider $2^{12} = 4096$ designs at each step. With the efficiency of the Wannier basis update, a through search can be done.

It is true that a better design may exist if we optimize the six enlargement regions together in one step. However, intuitively the step-by-step approach has a good chance of finding a good design. At each enlargement step, the tuning region is always perturbing the previous design and field pattern from one side only. Imagine moving the current tuning slice to the right away from the device region, then each enlargement step would be a isolated filter tuning the output of the mode separator. Stacks such filters (from the 6 tuning steps) are strong and commonly used modalities for tuning the output of a device, and we expect that the stacking of the filters close together will only do better. This close stacking is not explored before, because only the Wannier basis update approach can efficiently handle the strong interaction between the closely stacked filters.

Fig. 2(b) shows the device after optimization. On a 1-GHz Pentium III computer each update took about 3 s to compute. The final design is found in $\sim$24 hours of computer time, after searching through all 24 576 possible designs. We would like to emphasize the dramatic reduction in computational complexity of the method. If FDTD simulations are used, roughly 10 h would be needed on the same computer to find the change in the transmission for the addition or removal of one rod. Finding the optimized device, where we calculated the effect of tens of husbands of possible perturbation scenarios, would be extremely computationally expensive for FDTD. It should be pointed out that, before starting the optimization, we needed roughly 10 min of computation time to calculate the perturbation matrix $\delta\mathbf{D}$ for perturbation to a single unit cell. This matrix, however, only needs to be calculated once as we discussed in Section III-B.

Fig. 3 compares the device performance before and after optimization. We can see that the device characteristics, especially the transmission into the desired output at 1500 nm, are greatly improved compared to the initial design. Note that we have restricted our design space to the complete removal or addition of high index rods to the device region. The rods all have the same index and radius. Although arbitrary transmission characteristics are not always achievable, Fig. 3 shows that very good transmission characteristics can be obtained. Furthermore, the simple geometry makes the design much easier to fabricate.

Fig. 3 is obtained using the FDTD calculations. The FDTD result validated our Wannier basis analysis. At the design frequency, the transmission/reflection coefficients found using FDTD agree well with the Wannier basis calculations. Most importantly, the FDTD spectra show that even though we have optimized the transmission for a single frequency using our method, the resulting device has a working bandwidth of about 5 nm. This is because we have chosen the device enlargement regions to be next to each other, and made all defects in the device enlargement regions weakly confined. The fact that none of the defects will introduce sharp unwanted spectra features ensures our design will have a usable bandwidth. This is confirmed by the smooth spectra in Fig. 3. In other words, this method of enlarging the device could be controlled to generate designs without unwanted high-Q cavities, which potentially makes the designs more tolerant to fabrication errors.

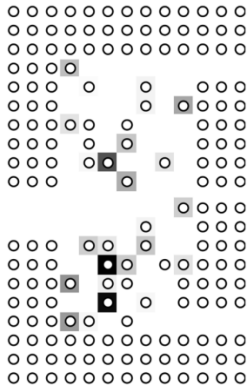

Fig. 4. Sensitivity of the transmission coefficients to dielectric perturbation of each individual rod. Darker shading around each rod represents a larger change to the sum of the squares of the wanted transmissions for the corresponding rod.

B. WBG Sensitivity Analysis

WBG provides a powerful and efficient means of performing sensitivity analysis for the mode separator designed in the previous section. Identifying the more sensitive regions in the device is of interest for understanding both device operation and fabrication. For the sake of demonstrating the analysis technique, we assume the dielectric constant of each rod is perturbed. We can now use (33) to calculate the derivative of the sum of the intended transmission power w.r.t. the index of each rod. Fig. 4 shows the result of the sensitivity calculation. From the figure we can readily identify regions of the device that are most sensitive to perturbations. By examining the field distribution, we can see that the most sensitive regions roughly match the regions with the highest field concentration. This provides an intuitive verification of our sensitivity analysis, and also suggests that, in design of photonic nanostructures for minimum sensitivity to variations in the structure, regions of high field concentration should be avoided if possible.

It should be pointed out that, if FDTD simulations are used, roughly 10 h would be needed on a Pentium III computer to find the change in the transmission for perturbation to just one single unit cell. Generating the sensitivity map in Fig. 2(a), where we calculated the effect of perturbing 33 individual rods, would be extremely computationally expensive for FDTD. In contrast, our WBG method took roughly 10 s to compute the whole sensitivity map. We also verified the WBG sensitivity calculation for resonators using the PWM method. The agreement is to three

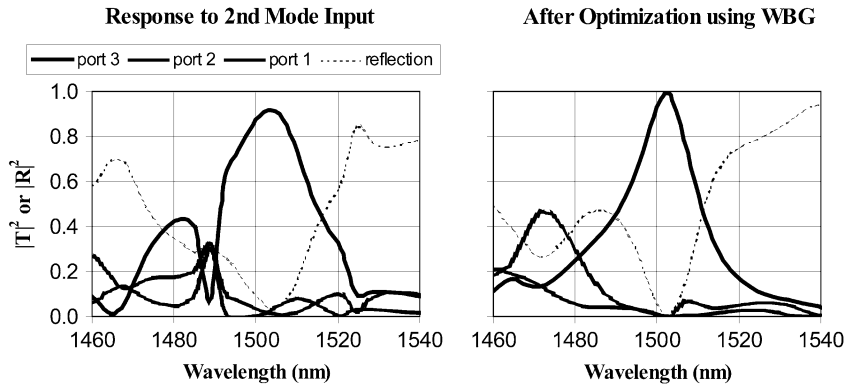

Fig. 5. FDTD transmission and reflection spectra before and after fine tuning using a combination of optimization based on sensitivity analysis and optimization based on small rank adjustment. The spectra are for the second-order input waveguide mode. Ports 1, 2, and 3 refer to the three output waveguides.

significant figures, with similar $\sim 1000\times$ calculation speed gain. If we need to search through a large number of designs for a given sensitivity criterion, using the WBG approach is the only available practical method known to the authors.

C. Systematic Device Design With Wannier Basis Local Optimization

We will again use the mode multiplexer to demonstrate the device design process with Wannier basis local optimization. As we can see from Fig. 3, the peak transmission through the original mode separator is around 90%. Ideally we would like to increase this figure to 100%. In this section, to further improve the transmission, we will fine-tune a large number of design parameters simultaneously. For the sake of this demonstration, we will try to fine-tune the dielectric constant of the remaining high index rods in the optimization region [see Fig. 2(a)]. There are 33 rods remaining in this region.

To find the sensitivity of the transmission w.r.t. the rod indices, we calculate three gradient vectors $dt_1/d\vec{\gamma}, dt_2/d\vec{\gamma}, dt_3/d\vec{\gamma}$, where t_m represents the transmission on the desired output for input mode m, and $\vec{\gamma} = \{\gamma_{\vec{\boldsymbol{R}}}, \vec{\boldsymbol{R}} = \boldsymbol{R}_1, \ldots, \boldsymbol{R}_{33}\}$ parameterizes the index change in the 33 rods. The fine-tuning involves modifying the structure in repeated steps, but because for all steps and for each rod, we will be only scaling the rod's dielectric constant, $\partial \mathbf{D}_{\delta,0}/\partial\gamma = \mathbf{D}_{R_i}$ only has to be calculated once. For this specific structure, $dt_1/d\vec{\gamma}, dt_2/d\vec{\gamma}, dt_3/d\vec{\gamma}$ can be calculated on a Pentium III computer in roughly 3 min. Our goal is to maximize $|t|^2 = |t_1|^2 + |t_2|^2 + |t_3|^2$. In this example, after finding the gradient of $|t|^2$, we use steepest descent to choose the modification to the 33 rods in each iteration. Each iteration takes roughly 3 min on a Pentium III computer, including the time to find the new transmission coefficients. The local optimum was found in roughly 500 iterations.

Fig. 5 shows the transmission spectrum before and after the optimization for the second-order mode. The spectrum is found using FDTD simulation in order to verify the result obtained using our Wannier based methods. Similar results are obtained for the other two modes. From Fig. 5 we can see that the peak transmission increased from 90% to nearly unity after the optimization. This example demonstrates that combining sensitivity analysis with small rank adjustment is a powerful tool for designing realistic functional devices.

Physically, changing the index of each rod poses a challenge to today's fabrication techniques. Changing the radius of the 33 rods in the optimization region may be easier from a fabrication standpoint. In our optimization, we presumed that we could tune the index continuously. We did not choose to modify the rod radii in this example for two reasons. First, changing the index is sufficient to demonstrate the idea of combining sensitivity analysis with low rank inverse adjustment. Second, fine-tuning the rod radius is a trivial task in the Wannier formulation, but simulating the resulting structure in FDTD would require extremely high-resolution computational grids. This would have made the verification of our final design much more troublesome. We expect changing the rod radius will achieve similar results as changing the index.

VII. Summary

We have presented a powerful general framework for designing PC devices by utilizing efficient optimization and sensitivity analysis techniques. We demonstrated that our Wannier-function-based global optimization can be used to design extremely compact PC devices with complex functionalities. In the design process, we analyze perturbed device characteristics exactly, without linearization approximations. Our optimization method probes large sets of discrete changes to a device with unprecedented speed and accuracy. This allows us to design useful devices even when there is little physical intuition to guide the initial guess of the device structure. Furthermore, we have shown that our sensitivity analysis method, due to its computational speed, can be used with our discrete update method to fine-tune the PC device designs.

Our sensitivity analysis of the mode separator empirically confirms the intuition that the areas with higher field concentration are the ones that lead to the highest sensitivity to fabrication variations. In future research, the objective function in our design optimization can be chosen to favor designs with relatively uniform field concentration throughout the structure, which will make the device designed using our method less sensitive to fabrication variations. The numerical examples here are presented in 2-D. The Wannier based design formalism, both the Wannier basis analysis and the optimization methods, can be generalized

to 3-D. For 2-D structures with finite thickness, such as high index slabs with air holes, the Wannier based design formalism can be applied easily when the radiation loss is negligible. With further research, we believe radiation loss can also be included in the Wannier basis device optimization as well, possibly using a matrix renormalization technique. We believe the methods in this paper will enable researchers to design compact PC devices with novel and complex functionalities.

APPENDIX

A. Vector Wave Equation in the Wannier Basis With Both Permittivity and Permeability Defects

We can further simplify the left-hand side of (3). For the periodic part, we get

$$\begin{aligned}
&\nabla\times\underline{\mu}_p(\boldsymbol{r})^{-1}\nabla\times\boldsymbol{E}(\boldsymbol{r})\\
&\quad=\nabla\times\underline{\mu}_p(\boldsymbol{r})^{-1}\nabla\times\sum_{n,\boldsymbol{R}}b_{n,\boldsymbol{R}}\boldsymbol{W}_{n,\boldsymbol{R}}(\boldsymbol{r})\\
&\quad=\nabla\times\underline{\mu}_p(\boldsymbol{r})^{-1}\nabla\times\sum_{n,\boldsymbol{R}}b_{n,\boldsymbol{R}}\frac{\Omega}{(2\pi)^3}\\
&\qquad\times\int_{\mathrm{BZ}}d\boldsymbol{k}e^{-i\boldsymbol{k}\cdot\boldsymbol{R}}\sum_m\left[\mathbf{U}^{(\boldsymbol{k})}_{n,m}\right]\boldsymbol{E}_m(\boldsymbol{k},\boldsymbol{r})\\
&\quad=\sum_{n,\boldsymbol{R}}b_{n,\boldsymbol{R}}\frac{\Omega}{(2\pi)^3}\int_{\mathrm{BZ}}d\boldsymbol{k}e^{-i\boldsymbol{k}\cdot\boldsymbol{R}}\\
&\qquad\times\sum_m\left[\mathbf{U}^{(\boldsymbol{k})}_{n,m}\right]\nabla\underline{\mu}_p(\boldsymbol{r})^{-1}\nabla\times\boldsymbol{E}_m(\boldsymbol{k},\boldsymbol{r})\\
&\quad=\sum_{n,\boldsymbol{R}}b_{n,\boldsymbol{R}}\frac{\Omega}{(2\pi)^3}\int_{\mathrm{BZ}}d\boldsymbol{k}e^{-i\boldsymbol{k}\cdot\boldsymbol{R}}\\
&\qquad\times\sum_m\left[\mathbf{U}^{(\boldsymbol{k})}_{n,m}\right]\omega_m^2(\boldsymbol{k})\underline{\varepsilon}_p(\boldsymbol{r})\boldsymbol{E}_m(k,r)
\end{aligned}\tag{39}$$

where we used (1) for the last line. The integral in (39) can be written as

$$\begin{aligned}
&\int_{\mathrm{BZ}}d\boldsymbol{k}e^{-i\boldsymbol{k}\cdot\boldsymbol{R}}\sum_m\left[\mathbf{U}^{(\boldsymbol{k})}_{n,m}\right]\omega_m^2(\boldsymbol{k})\underline{\varepsilon}_p(\boldsymbol{r})\boldsymbol{E}_m(\boldsymbol{k},\boldsymbol{r})\\
&\quad=\int_{\mathrm{BZ}}d\boldsymbol{k}e^{-i\boldsymbol{k}\cdot\boldsymbol{R}}\sum_m\left[\mathbf{U}^{(\boldsymbol{k})}_{n,m}\right]\omega_m^2(\boldsymbol{k})\underline{\varepsilon}_p(\boldsymbol{r})\\
&\qquad\times\sum_{\boldsymbol{R}'}e^{i\boldsymbol{k}\cdot\boldsymbol{R}'}\sum_{n'}\left[\mathbf{U}^{\dagger(\boldsymbol{k})}_{m,n'}\right]\boldsymbol{W}_{n',R'}(\boldsymbol{r})\\
&\quad=\sum_{n',\mathbf{R}'}\int_{\mathrm{BZ}}d\boldsymbol{k}e^{i\mathbf{k}\cdot(\boldsymbol{R}'-\boldsymbol{R})}\\
&\qquad\times\sum_m\left[\mathbf{U}^{(\boldsymbol{k})}_{n,m}\right]\omega_m^2(\boldsymbol{k})\left[\mathbf{U}^{\dagger(\boldsymbol{k})}_{m,n'}\right]\underline{\varepsilon}_p(\boldsymbol{r})\boldsymbol{W}_{n',\boldsymbol{R}'}(\boldsymbol{r})\\
&\quad\equiv\frac{(2\pi)^3}{\Omega}\sum_{n',\mathbf{R}'}[\mathbf{A}_{n'\boldsymbol{R}',n\boldsymbol{R}}]\underline{\varepsilon}_p(\boldsymbol{r})\boldsymbol{W}_{n',\boldsymbol{R}'}(\boldsymbol{r})
\end{aligned}$$

where we have defined the matrix elements $\mathbf{A}_{n'\boldsymbol{R}',n\boldsymbol{R}}$, in the last line. Putting this back into (39), we get

$$\begin{aligned}
&\nabla\times\underline{\mu}_p(\boldsymbol{r})^{-1}\nabla\times\boldsymbol{E}(\boldsymbol{r})\\
&\qquad=\sum_{n,\boldsymbol{R}}b_{n,\boldsymbol{R}}\sum_{n',\mathbf{R}'}[\mathbf{A}_{n'\boldsymbol{R}',n\boldsymbol{R}}]\underline{\varepsilon}_p(\boldsymbol{r})\boldsymbol{W}_{j,\boldsymbol{R}'}(\boldsymbol{r}).
\end{aligned}\tag{40}$$

Multiplying (40) by $\boldsymbol{W}^{\dagger}_{n'',\boldsymbol{R}''}(\boldsymbol{r})$ and integrating

$$\begin{aligned}
&\int d\boldsymbol{r}\boldsymbol{W}^{\dagger}_{n'',\boldsymbol{R}''}(\boldsymbol{r})\nabla\times\underline{\mu}_p(\boldsymbol{r})^{-1}\nabla\times\boldsymbol{E}(\boldsymbol{r})\\
&\quad=\sum_{n,\boldsymbol{R}}b_{n,\boldsymbol{R}}\sum_{n',\mathbf{R}'}[\mathbf{A}_{n'\boldsymbol{R}',n,\boldsymbol{R}}]\\
&\qquad\times\int d\boldsymbol{r}\boldsymbol{W}^{\dagger}_{n'',\boldsymbol{R}''}(\boldsymbol{r})\underline{\varepsilon}_p(\boldsymbol{r})\boldsymbol{W}_{n',\boldsymbol{R}'}(\boldsymbol{r})\\
&\quad=\sum_{n,\boldsymbol{R}}[\mathbf{A}_{n''\boldsymbol{R}'',\boldsymbol{n}R}]b_{n,\boldsymbol{R}}
\end{aligned}\tag{41}$$

where we have used the orthogonality of the Wannier functions.

The defect term in (2) for the permeability leads to

$$\begin{aligned}
&\int_{\mathbb{R}}d\boldsymbol{r}\boldsymbol{W}^*_{n",\boldsymbol{R}"}(\boldsymbol{r})\cdot\nabla\times\underline{\eta}(\boldsymbol{r})\nabla\times\boldsymbol{E}(\boldsymbol{r})\\
&\quad=\sum_{n,\boldsymbol{R}}b_{n,\boldsymbol{R}}\int_{\mathbb{R}}d\boldsymbol{r}\boldsymbol{W}^*_{n",\boldsymbol{R}"}(\boldsymbol{r})\\
&\qquad\cdot\nabla\times\underline{\eta}(\boldsymbol{r})\nabla\times\boldsymbol{W}_{n,\boldsymbol{R}}(\boldsymbol{r})\\
&\quad=\sum_{n,\boldsymbol{R}}b_{n,\boldsymbol{R}}\int_{\mathbb{R}}d\boldsymbol{r}\nabla\times\boldsymbol{W}^*_{n,\boldsymbol{R}}(\boldsymbol{r})\\
&\qquad\cdot\underline{\eta}^*(\boldsymbol{r})\nabla\times\boldsymbol{W}_{n'',\boldsymbol{R}''}(\boldsymbol{r})\\
&\qquad-\nabla\cdot[\boldsymbol{W}^*_{n'',\boldsymbol{R}''}(\boldsymbol{r})\times\underline{\eta}(\boldsymbol{r})\nabla\times\boldsymbol{W}_{n,\boldsymbol{R}}(\boldsymbol{r})]
\end{aligned}$$

where we used the vector identity $\boldsymbol{a}\cdot\nabla\times\boldsymbol{b}=\boldsymbol{b}\cdot\nabla\times\boldsymbol{a}-\nabla\cdot(\boldsymbol{a}\times\boldsymbol{b})$. Using Gauss's theorem on the second term in the integral, and the fact that the Wannier functions approach zero quickly enough at infinity, the second term vanishes. Defining the rest of the integral as the permeability defect matrix element

$$\mathbf{B}_{n''\boldsymbol{R}'',n\boldsymbol{R}}\equiv\int_{\mathbb{R}}d\boldsymbol{r}\nabla\times\boldsymbol{W}^*_{n,\boldsymbol{R}}(\boldsymbol{r})\cdot\underline{\eta}^*(\boldsymbol{r})\nabla\times\boldsymbol{W}_{n'',\boldsymbol{R}''}(\boldsymbol{r})$$

we get

$$\begin{aligned}
&\int_{\mathbb{R}}d\boldsymbol{r}\boldsymbol{W}^*_{n'',\boldsymbol{R}''}(\boldsymbol{r})\cdot\nabla\times\underline{\eta}(\boldsymbol{r})\nabla\times\boldsymbol{E}(\boldsymbol{r})\\
&\qquad=\sum_{n,\boldsymbol{R}}[\mathbf{B}_{n''\boldsymbol{R}'',n\boldsymbol{R}}]b_{n,\boldsymbol{R}}.
\end{aligned}\tag{42}$$

The right-hand side of (3) is somewhat simpler to expand in the Wannier basis

$$\begin{aligned}
&\int_{\mathbb{R}}d\boldsymbol{r}\boldsymbol{W}^*_{n'',\boldsymbol{R}''}(\boldsymbol{r})\cdot\omega^2\underline{\varepsilon}(\boldsymbol{r})\boldsymbol{E}(\boldsymbol{r})\\
&\quad=\omega^2\sum_{n,\boldsymbol{R}}b_{n,\boldsymbol{R}}\int_{\mathbb{R}}d\boldsymbol{r}\boldsymbol{W}^*_{n'',\boldsymbol{R}''}(\boldsymbol{r})\cdot\underline{\varepsilon}(\boldsymbol{r})\boldsymbol{W}_{n,\boldsymbol{R}}(\boldsymbol{r})\\
&\quad=\omega^2\sum_{n,\boldsymbol{R}}b_{n,\boldsymbol{R}}\left[\delta_{nn''}\delta_{\boldsymbol{R}R''}\right.\\
&\qquad\left.+\int_{\mathbb{R}}d\boldsymbol{r}\boldsymbol{W}^*_{n'',\boldsymbol{R}''}(\boldsymbol{r})\cdot\underline{\varepsilon}_{\Delta}(\boldsymbol{r})\boldsymbol{W}_{n,\boldsymbol{R}}(\boldsymbol{r})\right]
\end{aligned}$$

where we used the orthogonality of the Wannier basis functions in the last step. Defining the integral term as the permittivity defect matrix element

$$\mathbf{D}_{n''\boldsymbol{R}'',n\boldsymbol{R}}\equiv\int_{\mathbb{R}}d\boldsymbol{r}\boldsymbol{W}^*_{n'',\boldsymbol{R}''}(\boldsymbol{r})\cdot\underline{\varepsilon}_{\Delta}(\boldsymbol{r})\boldsymbol{W}_{n,\boldsymbol{R}}(\boldsymbol{r})\tag{43}$$

we get

$$\int_{\mathbb{R}} d\boldsymbol{r}\boldsymbol{W}^*_{n'',\boldsymbol{R}''}(\boldsymbol{r})\cdot\omega^2\underline{\varepsilon}(\boldsymbol{r})\boldsymbol{E}(\boldsymbol{r}) = \omega^2\sum_{n,\boldsymbol{R}} b_{n,\boldsymbol{R}}[\delta_{n''n}\delta_{\boldsymbol{R}''\boldsymbol{R}} + \mathbf{D}_{n''\boldsymbol{R}'',n\boldsymbol{R}}] \quad (44)$$

where δ_{nm} is the Kronecker delta. Combining (44), (42), and (41), we get the Wannier basis system equation

$$\sum_{n,\boldsymbol{R}}[\mathbf{B}_{n''\boldsymbol{R}'',n\boldsymbol{R}} - \omega^2\mathbf{D}_{n''\boldsymbol{R}'',n\boldsymbol{R}}]b_{n,\boldsymbol{R}} = \sum_{n,\boldsymbol{R}}[\omega^2\delta_{n''n}\delta_{\boldsymbol{R}''\boldsymbol{R}} - \mathbf{A}_{n''\boldsymbol{R}'',n\boldsymbol{R}}]b_{n,\boldsymbol{R}}. \quad (45)$$

To simplify notation, we will write the set of Wannier basis coefficients in vector form: $\mathbf{b} \equiv \{b_{n,\boldsymbol{R}}\}$. Now (45) can be written in the form

$$[\mathbf{B} - \omega^2\mathbf{D}]\mathbf{b} = [\omega^2\mathbf{I} - \mathbf{A}]\mathbf{b} \quad (46)$$

where $\mathbf{I}$ is the identity matrix, and each dimension of the matrices are indexed by both n and R.

B. Small Rank Adjustment to the Inverse

The small rank adjustment to the inverse is also known as Matrix Inversion Lemma or the Sherman–Morrison–Woodbury formula. A derivation is provided below for reference. For square matrices $\mathbf{F}$ and $\mathbf{D}$, assume $\mathbf{D}$ can be written as $\mathbf{D} = \mathbf{XHY}$, where $\mathbf{X}$ is a skinny (a rectangular matrix with a longer vertical dimension), $\mathbf{H}$ is square, $\mathbf{Y}$ is fat (longer horizontal dimension), and $\mathbf{H}$ is full rank. Given $\mathbf{F}^{-1}$, we wish to find $(\mathbf{F}+\mathbf{D})^{-1}$. Let $\Lambda = \mathbf{F} + \mathbf{D}$, we have

$$\begin{aligned}\Lambda^{-1}\Lambda &= \mathbf{I}\\ \mathbf{I} &= \Lambda^{-1}\mathbf{F} + \Lambda^{-1}\mathbf{XHY}\\ \mathbf{F}^{-1} &= \Lambda^{-1} + \Lambda^{-1}\mathbf{XHYF^{-1}}\\ \mathbf{F}^{-1} - \Lambda^{-1} &= \Lambda^{-1}\mathbf{XHYF}^{-1}.\end{aligned} \quad (47)$$

Multipling the third line of (47) by $\mathbf{X}$, we have

$$\begin{aligned}\mathbf{F}^{-1}\mathbf{X} &= \Lambda^{-1}\mathbf{X} + \Lambda^{-1}\mathbf{XHYF}^{-1}\mathbf{X}\\ &= \Lambda^{-1}\mathbf{XH}(\mathbf{H}^{-1} + \mathbf{YF}^{-1}\mathbf{X})\\ \Lambda^{-1}\mathbf{XH} &= \mathbf{F}^{-1}\mathbf{X}(\mathbf{H}^{-1} + \mathbf{YF}^{-1}\mathbf{X})^{-1}\\ \Lambda^{-1}\mathbf{XHYF}^{-1} &= \mathbf{F}^{-1}\mathbf{X}(\mathbf{H}^{-1} + \mathbf{YF}^{-1}\mathbf{X})^{-1}\mathbf{YF}^{-1}.\end{aligned} \quad (48)$$

Now substitute (48) into the last line of (47); we have

$$\Lambda^{-1} = \mathbf{F}^{-1} - \mathbf{F}^{-1}\mathbf{X}(\mathbf{H}^{-1} + \mathbf{YF}^{-1}\mathbf{X})^{-1}\mathbf{YF}^{-1}. \quad (49)$$

Now if we substitute $\mathbf{X}$ with $\mathbf{XV}$ and $\mathbf{Y}$ with $\mathbf{WY}$ in (49), we get (20).

C. Sensitivity for Generalized Eigenvalue

Reference [15] has given a sensitivity equation for classical eigenvalues; here we generalize it to generalized eigenvalues. Let $\beta(\gamma)$ be an nondegenerate generalized eigenvalue of any two matrices $\mathbf{A}, \mathbf{B}$, then the generalized eigenvalue equations are

$$\begin{aligned}\mathbf{Av} &= \beta\mathbf{Bv}\\ \mathbf{w}^\dagger\mathbf{A} &= \beta\mathbf{w}^\dagger\mathbf{B}\end{aligned} \quad (50)$$

where $\mathbf{v}$ and $\mathbf{w}$ are the right and left eigenvectors of $\mathbf{A}, \mathbf{B}$ associated with $\beta(\gamma)$. Multiplying the first equation by $\mathbf{w}^\dagger$, we get

$$\frac{\mathbf{w}^\dagger\mathbf{Av}}{\beta} = \mathbf{w}^\dagger\mathbf{Bv}.$$

Equivalently, we can write β as

$$\beta = \frac{\mathbf{w}^\dagger\mathbf{Av}}{\mathbf{w}^\dagger\mathbf{Bv}}.$$

Taking the derivative of the above expression w.r.t γ, we get

$$\frac{d\beta}{d\gamma} = \frac{-\mathbf{w}^\dagger\mathbf{Av}}{(\mathbf{w}^\dagger\mathbf{Bv})^2}\left(\frac{d\mathbf{w}^\dagger}{d\gamma}\mathbf{Bv} + \mathbf{w}^\dagger\frac{d\mathbf{B}}{d\gamma}\mathbf{v} + \mathbf{w}^\dagger\mathbf{B}\frac{d\mathbf{v}}{d\gamma}\right) + \frac{1}{\mathbf{w}^\dagger\mathbf{Bv}}\left(\frac{d\mathbf{w}^\dagger}{d\gamma}\mathbf{Av} + \mathbf{w}^\dagger\frac{d\mathbf{A}}{d\gamma}\mathbf{v} + \mathbf{w}^\dagger\mathbf{A}\frac{d\mathbf{v}}{d\gamma}\right). \quad (51)$$

Substituting (50) into (51), we get

$$\begin{aligned}\frac{d\beta}{d\gamma} &= \frac{-\mathbf{w}^\dagger\mathbf{Av}}{(\mathbf{w}^\dagger\mathbf{Bv})^2}\times\left(\frac{1}{\beta}\frac{d\mathbf{w}^\dagger}{d\gamma}\mathbf{Av} + \mathbf{w}^\dagger\frac{d\mathbf{B}}{d\gamma}\mathbf{v} + \frac{1}{\beta}\mathbf{w}^\dagger\mathbf{A}\frac{d\mathbf{v}}{d\gamma}\right)\\ &\quad + \frac{1}{\mathbf{w}^\dagger\mathbf{Bv}}\left(\frac{d\mathbf{w}^\dagger}{d\gamma}\mathbf{Av} + \mathbf{w}^\dagger\frac{d\mathbf{A}}{d\gamma}\mathbf{v} + \mathbf{w}^\dagger\mathbf{A}\frac{d\mathbf{v}}{d\gamma}\right)\\ &= \frac{1}{\mathbf{w}^\dagger\mathbf{Bv}}\left(\mathbf{w}^\dagger\frac{d\mathbf{A}}{d\gamma}\mathbf{v} - \beta\mathbf{w}^\dagger\frac{d\mathbf{B}}{d\gamma}\mathbf{v}\right).\end{aligned} \quad (52)$$

Replacing $\mathbf{A}$ by $\mathbf{I} + \mathbf{D} + \mathbf{D}_{\delta,0}(\gamma)$ and $\mathbf{B}$ by $\mathbf{A} + \mathbf{B}$, and using the fact that we assume $\mathbf{A} + \mathbf{B}$ do not change with γ (i.e., no magnetic defects), we get the WBG resonator sensitivity equation.

ACKNOWLEDGMENT

Y. Jiao, the first author, would like to thank W. Zheng and X. Liu for insightful discussions during the development of this work.

REFERENCES

[1] A. Taflove and S. C. Hagness, "Computational electrodynamics: The finite-difference time-domain method," in *Artech House Antennas and Propagation Library*, 2nd ed. Boston, MA: Artech House, 2000.

[2] S. G. Johnson and J. D. Joannopoulos, "Block-iterative frequency-domain methods for Maxwell's equations in a planewave basis," *Opt. Exp.*, vol. 8, no. 3, pp. 173–190, 2001.

[3] R. Wilson, T. J. Karle, I. Moerman, and T. F. Krauss, "Efficient photonic crystal Y-junctions," *J. Opt. A: Pure Appl. Opt.*, vol. 5, no. 4, pp. S76–80, 2003.

[4] J. Vuckovic, M. Loncar, H. Mabuchi, and A. Scherer, "Optimization of the Q factor in photonic crystal microcavities," *IEEE J. Quantum Electron.*, vol. 38, no. 7, pp. 850–856, Jul. 2002.

[5] E. Moreno, D. Erni, and C. Hafner, "Modeling of discontinuities in photonic crystal waveguides with the multiple multipole method—Art. no. 036 618," *Phys. Rev. E*, vol. 66, no. 3, 2002. p. 036 618.

[6] K. Ohtaka and Y. Tanabe, "Photonic band using vector spherical waves: 1. Various properties of Bloch electric fields and heavy photons," *J. Phys. Soc. Jpn.*, vol. 65, no. 7, pp. 2265–2275, 1996.

[7] Z. Y. Li and K. M. Ho, "Light propagation in semi-infinite photonic crystals and related waveguide structures," *Phys. Rev. B*, vol. 68, no. 15, p. 155 101, 2003.

[8] G. Veronis, R. W. Dutton, and S. H. Fan, "Method for sensitivity analysis of photonic crystal devices," *Opt. Lett.*, vol. 29, no. 19, pp. 2288–2290, 2004.

[9] N. Marzari and D. Vanderbilt, "Maximally localized generalized Wannier functions for composite energy bands," *Phys. Rev. B*, vol. 56, no. 20, pp. 12 847–12 865, 1997.

[10] K. Busch, S. F. Mingaleev, A. Garcia-Martin, M. Schillinger, and D. Hermann, "The Wannier function approach to photonic crystal circuits," *J. Phys.: Condensed Matter*, vol. 15, no. 30, pp. R1233–56, 2003.
[11] J. P. Albert, C. Jouanin, D. Cassagne, and D. Bertho, "Generalized Wannier function method for photonic crystals," *Phys. Rev. B*, vol. 61, no. 7, pp. 4381–4384, 2000.
[12] Y. Jiao, S. H. Fan, and D. A. B. Miller, "Demonstration of systematic photonic crystal device design and optimization by low-rank adjustments: An extremely compact mode separator," *Opt. Lett.*, vol. 30, no. 2, pp. 141–143, 2005.
[13] Y. Jiao, S. Fan, and D. A. B. Miller, "Photonic crystal defect sensitivity analysis with Wannier basis gradients," *Opt. Lett.*, vol. 30, no. 3, pp. 302–304, 2005.
[14] K. M. Leung, "Defect modes in photonic band structures—A green-function approach using Vector Wannier functions," *J. Opt. Soc. Amer. B*, vol. 10, no. 2, pp. 303–306, 1993.
[15] R. A. Horn and C. R. Johnson, *Matrix Analysis*. Cambridge, U.K.: Cambridge Univ. Press, 1990, p. 561.
[16] S. G. Johnson, M. Ibanescu, M. A. Skorobogatiy, O. Weisberg, J. D. Joannopoulos, and Y. Fink, "Perturbation theory for Maxwell's equations with shifting material boundaries," *Phys. Rev. E*, vol. 65, no. 6, pp. 066 611–7, 2002.
[17] S. Boyd and L. Vandenberghe, *Convex Optimization*. Cambridge, U.K.: Cambridge Univ. Press, 2004.
[18] K. Schittkowski, "NLQPL: A FORTRAN-subroutine solving constrained nonlinear programming problems," *Ann. Operations Res.*, vol. 5, pp. 485–500, 1985.
[19] B. T. Lee and S. Y. Shin, "Mode-order converter in a multimode waveguide," *Opt. Lett.*, vol. 28, no. 18, pp. 1660–1662, 2003.
[20] J. Leuthold, J. Eckner, E. Gamper, P. A. Besse, and H. Melchior, "Multimode interference couplers for the conversion and combining of zeroth and first-order modes," *J. Lightw. Technol.*, vol. 16, no. 7, pp. 1228–39, Jul. 1998.

Yang Jiao (M'96) received the B.S. degree in electrical engineering and computer science from the University of California at Berkeley in 2000. He received the M.S. and Ph.D. degrees in electrical engineering from Stanford University, Stanford, CA, in 2002 and 2005, respectively. His thesis research focused on systematic and efficient methods for the analysis, design, and optimization of nanophotonic devices.

His research interests are in theoretical, computational, and experimental studies of nano-scale structures and devices, including photonic crystals, microcavities, plasmonics, nanowires, and nanophotonic circuits and elements. He is currently with Intel Corporation, Santa Clara, CA.

Dr. Jiao is a recipient of the National Science Foundation Graduate Student Research Fellowship and the Stanford Graduate Student Fellowship from 2000 to 2004.

Shanhui Fan received the Ph.D. degree in 1997 in theoretical condensed matter physics from the Massachusetts Institute of Technology (MIT), Cambridge.

He has been an Assistant Professor of electrical engineering at Stanford University since 2001. He was a Research Scientist at the Research Laboratory of Electronics at MIT prior to his appointment at Stanford. His research interests are in computational and theoretical studies of solid-state and photonic structures and devices, especially photonic crystals, microcavities, and nanophotonic circuits and elements. He has published more than 60 journal articles in this field, has given more than 40 invited talks at major international conferences, and currently holds 14 U.S. patents.

Prof. Fan is a recipient of the National Science Foundation Career Award in 2002, and a David and Lucile Packard Fellowship in Science and Engineering in 2003.

David A. B. Miller (M'84-SM'89-F'95) received the B.Sc. degree from St. Andrews University, Fife, U.K., and the Ph.D. degree from Heriot-Watt University, Edinburgh, U.K., in 1979.

He was with Bell Laboratories, Holmdel, NJ, from 1981 to 1996, as a Department Head from 1987, later of the Advanced Photonics Research Department. He is currently the W. M. Keck Professor of Electrical Engineering at Stanford University, Stanford, CA, and the Director of the Ginzton and Solid State and Photonics Laboratories, Stanford, CA. He has published more than 200 scientific papers, and holds over 55 patents. His research interests include quantum-well optoelectronic and nanophotonic physics and devices, and fundamental and applications of optics in information, sensing, switching, and processing.

Dr. Miller has served as a Board Member for both the Optical Society of America (OSA) and IEEE Lasers and Electro-Optics Society (LEOS), and in various other society and conference committees. He was President of the IEEE LEOS in 1995. He was awarded the Adolph Lomb Medal and the R. W. Wood Prize from the OSA, the International Prize in Optics from the International Commission for Optics, and the IEEE Third Millennium Medal. He is a Fellow of the Royal Societies of London and Edinburgh, U.K., Optical Society of America (OSA), and the American Physical Society, and holds an honorary degree from the Vrije Universiteit Brussel and Heriot-Watt University.